UHASSELT
KNOWLEDGE IN ACTION

Maastricht University

Faculty of Medicine and Life Sciences
School for Life Sciences
Master of Biomedical Sciences

Master's thesis

Lipid metabolism modulation during human Schwann cell differentiation for CMT1A therapy

Yara Lambrechts

Thesis presented in fulfillment of the requirements for the degree of Master of Biomedical Sciences, specialization Molecular Mechanisms in Health and Disease

SUPERVISOR :

Prof. dr. Esther WOLFS

MENTOR :

De heer Koen KUIPERS

2023
2024

Transnational University Limburg is a unique collaboration of two universities in two countries: the University of Hasselt and Maastricht University.

UHASSELT
KNOWLEDGE IN ACTION

www.uhasselt.be
Universiteit Hasselt
Campus Hasselt:
Martelarenlaan 42 | 3500 Hasselt
Campus Diepenbeek:
Agoralaan Gebouw D | 3590 Diepenbeek

Faculty of Medicine and Life Sciences
School for Life Sciences
Master of Biomedical Sciences

Master's thesis

Lipid metabolism modulation during human Schwann cell differentiation for CMT1A therapy

Yara Lambrechts

Thesis presented in fulfillment of the requirements for the degree of Master of Biomedical Sciences, specialization Molecular Mechanisms in Health and Disease

SUPERVISOR :

Prof. dr. Esther WOLFS

MENTOR :

De heer Koen KUIPERS

Lipid metabolism modulation during human Schwann cell differentiation for CMT1A therapy *

Lambrechts Y.[1], Kuipers K.[1], Vangansewinkel T.[1], Jeurissen H.[1], Vanherle S.[2], Dehaes K.[1]
*Bogie J.[2] and *Wolfs E.[1]

[1] Department of Cardio and Organ Systems, FIERCE lab, Biomedical Research Institute, Hasselt University, Agoralaan Gebouw C - B-3590 Diepenbeek, Belgium.
[2] Department of Immunology, BOGIE lab, Biomedical Research Institute, Hasselt University, Agoralaan Gebouw C - B-3590 Diepenbeek, Belgium.
*Shared last author.

*Running title: *Lipid metabolism modulation in CMT1A Schwann cells*

To whom correspondence should be addressed: Prof. dr. Esther Wolfs, Tel: +32 (11) 26 92 96; Email: esther.wolfs@uhasselt.be

Keywords: induced pluripotent stem cell (iPSC), Schwann cell (SC), lipid metabolism, Charcot-Marie-Tooth disease type 1A (CMT1A), ATP binding cassette subfamily A1 (ABCA1)

ABSTRACT

Charcot-Marie-Tooth disease type 1A (CMT1A) is a prevalent inherited peripheral neuropathy caused by a duplication of the Peripheral Myelin Protein 22 (PMP22) gene, leading to dysfunctional Schwann cells (SC) and impaired motor and sensory functions. The myelin sheath, which surrounds axons and enables saltatory conduction in the peripheral nervous system, consists of approximately 70% lipids. Hence, understanding lipid metabolism alterations and their effect on SC differentiation in CMT1A is essential for therapeutic drug development. This study aimed to investigate these aspects using CMT1A patient-derived induced pluripotent stem cells, differentiated into Schwann cell precursors (iPSC-SCP). The expression levels of SC differentiation markers in ISO and CMT1A iPSC-SCP and iPSC-immature SC were examined on gene and protein levels under lipid metabolism-altering conditions. These conditions showed varying effects on SC differentiation marker expression. Additionally, RNA-sequencing data of CMT1A SC revealed a significant increase of the cholesterol-efflux transporter, ATP binding cassette subfamily A1 (ABCA1), suggesting reduced intracellular cholesterol levels. Therefore, iPSC-SCP were exposed to an ABCA1 inhibitor, which positively impacted SC differentiation marker expression. These findings highlight ABCA1 inhibition as a potential therapeutic approach to rebalance cholesterol homeostasis and enhance SC differentiation. Overall, lipid modulation beneficially influenced CMT1A SC differentiation, necessitating further investigation. The modulation of SC lipid metabolism presents a promising avenue for therapeutic intervention in CMT1A by restoring dysfunctional Schwann cells.

INTRODUCTION

The diversity of CMT – Charcot-Marie-Tooth disease (CMT) has an estimated prevalence of 1 in 2500 and represents a diverse cluster of inherited peripheral nerve disorders, weaving its impact through axons and Schwann cells (SC) (1, 2). In 1886, Jean-Martin Charcot and his student Pierre Marie, along with Henry Tooth, independently marked the classification of hereditary motor and sensory neuropathy (HMSN), now synonymous with their names Charcot-Marie-Tooth (3). The disease manifests through a gradual progression of muscular atrophy, predominantly commencing in the lower extremities and subsequently affecting the upper extremities after several years. Distinctive features include fibrillations, cramps in atrophied muscles, and sensory impairments (4). CMT is classified traditionally based on nerve conduction velocities (NCV), with the mode of inheritance discerned through familial history and an additional genetic test for precise subtype diagnosis (5, 6).

CMT types are further delineated into demyelinating type 1 (CMT1), characterized by significantly reduced saltatory conduction

(NCV < 35 m/s), and axonal type 2 (CMT2), characterized by normal saltatory conduction (NCV > 45 m/s). CMTX represents an additional subtype with intermediate NCV (35-45 m/s), showcasing a relatively standard CMT phenotype (6). Despite the clinical similarities among patients with CMT, it is evident that the disorder is genetically heterogeneous (7). Subtypes (CMT1A, 2B, X1, etc.) are only given when the genetic cause is known, and each subtype corresponds to a specific gene (8). In most cases, CMT is inherited in an autosomal dominant manner, although there are also instances of recessive and X-linked forms (9).

CMT subtype 1A – Within this spectrum, Charcot-Marie-Tooth disease type 1A (CMT1A) emerges as the predominant subtype, representing 70-80% of all CMT1 cases and ranking as the most prevalent inherited peripheral neuropathy worldwide, with an incidence of 1 in 5,000 (10). Although CMT1A is primarily associated with genetic inheritance of the 1.5 megabase (Mb) duplication, sporadic occurrences due to *de novo* mutations have also been reported (11, 12). The duplicated region harbors the *Peripheral Myelin Protein 22 (PMP22)* gene, which is pivotal for myelin sheath formation and is recognized as the cause of CMT1A. This genetic aberration induces progressive demyelination or dysmyelination, primarily attributed to SC impairment (13, 14). In CMT1A, this results in motor and sensory impairments, manifesting as muscle cramps, tremors, and distal weakness, with symptoms typically becoming apparent during adolescence or early adulthood (13, 15-17).

The origin of Schwann cells – Schwann cells (SC) produce and maintain the myelin sheath around peripheral nerve fibers (18). The SC lineage arises from the neural crest, a multipotent stem cell population of ectodermal origin specific to vertebrate embryonal development (19, 20). Their induction and specification are primarily mediated by four major developmental pathways, i.e., *Wnt*, *FGF*, *BMP*, and *Notch* signaling (21). After the neural tube closes, premigratory neural crest cells experience an epithelial-to-mesenchymal transition (EMT). This transition enables them to detach from the neuroepithelium and migrate through the embryonal tissue. As dorsoventrally migrating neural crest cells connect with developing peripheral nerves and become Schwann cell precursors (SCP), both neural crest cells and SCP follow dedicated migration pathways to reach their target tissues, where they undergo differentiation towards their ultimate fate (22, 23).

The development of SCP into immature Schwann cells (iSC) involves intermediate stages (Fig. 1). This transformation coincides with the alteration of associated nerves, transitioning from a densely packed to a more relaxed structure facilitated by incorporating an extracellular matrix (24). While iSC, like SCP, stay closely associated with nerve axons, a key difference is that iSC start forming the basal lamina, a characteristic that remains in mature SC (23). Subsequently, the fate of iSC depends upon the type of axons with which they associate. iSC that are in contact with 'large-diameter' axons undergo radial sorting dependent on *neuregulin 1 (Nrg1)* expression levels, in which they increase their proliferation and form a 1:1 ratio with these axons and proceed to develop into mature myelinating SC (25, 26). Myelination and terminal differentiation involve the activation of laminin-211 *(Lama2)* and laminin-411 *(Lama4)*. These receptors signal the downstream regulator of myelination onset, *Krox20*, through cAMP-dependent protein kinase (PKA) activation, which regulates the expression of myelin-associated genes *myelin basic protein* (*MBP)* and *myelin protein zero* (*MPZ)* (27, 28). Yet, SC differentiation is reversible, and these cells show a high level of plasticity. In response to nerve injury, mature SC can re-enter the cell cycle, de-differentiate, and switch to the repair *Bungner* phenotype (29, 30). Conversely, iSC associated with several 'small-diameter' axons develop into mature non-myelinating Remak Schwann cells, wrapping them in Remak bundles without producing myelin (Fig. 1). However, the differential mechanisms specifying mature non-myelinating fates are largely unclear (25).

Identifying Schwann cells - To identify SC, three methods are commonly employed: the detection of specific markers, cell morphology assessment, and co-culture with dorsal root ganglion neurons to assess interactions with axons (7). Among these methods, the presence of specific markers is the most straightforward and widely used indicator for SC identification. Due to their plasticity, SC subpopulations are very heterogeneous. These subpopulations possess various shared and unique markers that can be used for identification purposes. Prior studies have uncovered several SC-specific

markers, with the most commonly utilized including *MBP*, *MPZ*, *P75^{NTR}*, *NCAM*, *Sox10*, *Oct6*, *Krox20*, and *Sox2* (Supplementary Table 2). However, relying solely on a few specific markers for identifying *in vitro* cultured iPSC-derived SC-like cells may pose limitations in reliability (31). Hence, one objective of this study was to purify the heterogeneous cell population using MACS to distinguish and target SCP from undifferentiated cells. This approach aims to achieve a more uniform cell distribution. If MACS proves effective, it could be integrated into the differentiation protocol to enhance the interpretability of future data.

Schwann cells in CMT1A – Given the abnormal myelination observed in peripheral nerves of CMT1A patients, SC lipid metabolism emerges as a potential key factor in the pathogenesis of the condition. Myelin lipids are essential for both the growth and long-term integrity of the myelin sheath. Approximately 70% of the myelin sheath consists of lipids, with phospholipids, cholesterol, and glycosphingolipids being the most abundant, comprising 50.6%, 27.2%, and 17% of the total lipids in purified PNS myelin, respectively (32). Research by *Fledrich et al.* demonstrated reduced lipid incorporation into myelin in a CMT1A rat model, resulting in an imbalance between myelin proteins and lipids, leading to alterations in the myelin sheath (32-34). Furthermore, studies in mice have shown impaired differentiation of SC contributing to the disease (35). However, the critical identification and functional understanding of the factors primarily responsible for the myelin and differentiation impairment in CMT1A remain elusive, representing a pivotal gap in unraveling the pathogenesis of CMT1A neuropathy (34).

Lipid metabolic abnormalities – In CMT1A, SC exhibit a notable transcriptional deficiency in genes related to lipid biosynthesis (32, 34). This disrupted lipid metabolism adversely impacts peripheral nerve physiology and myelin structure. However, the specific lipid species primarily responsible for the myelin impairment in CMT1A remain unidentified (34). Previous research demonstrated that modulating pathways associated with SC lipid metabolism showed promise in improving myelin formation and nerve function in CMT1A dorsal root ganglia (DRG) cultures and rodent models (30, 31). Nevertheless, data on lipid metabolism modulation using human *in vitro* models is currently lacking.

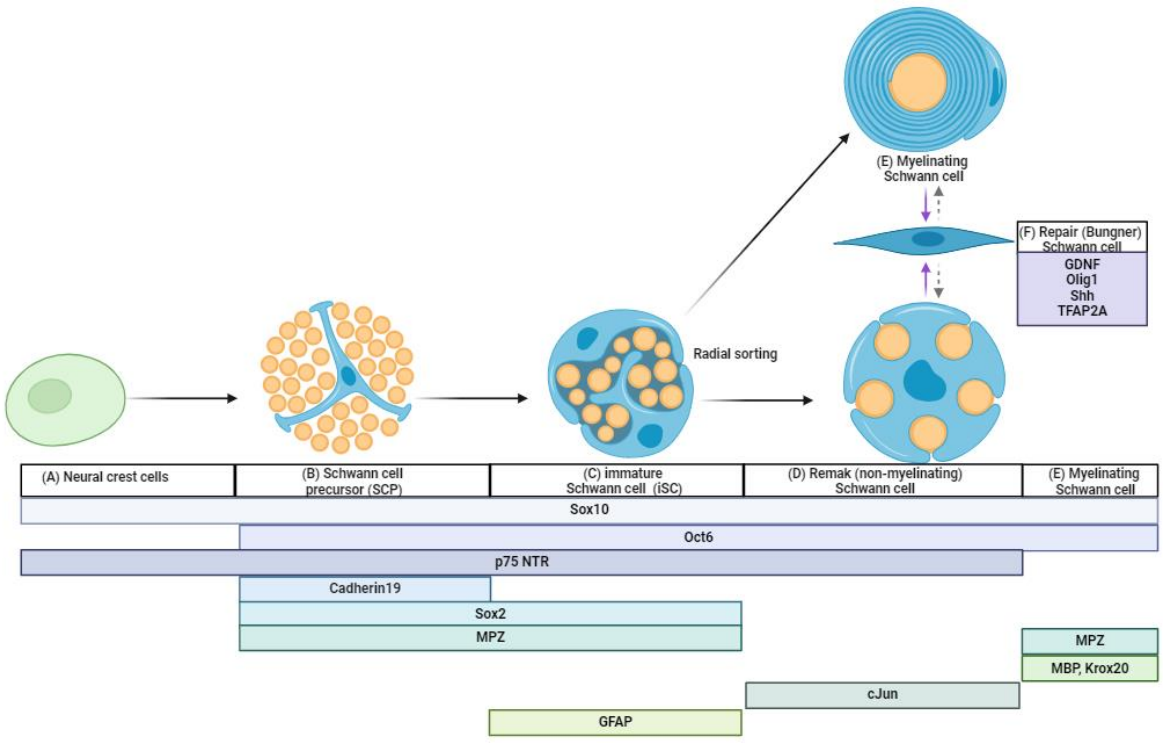

Figure 1: Schwann cell lineage. Illustration of the key cell types involved in Schwann cell development, and in nerve repair. Purple arrows; SC injury response; stippled arrows; post-repair formation of myelin and Remak cells. The figure was created with BioRender and adapted from (1).

Research has revealed that cholesterol biosynthesis is the main canonical pathway downregulated in CMT1A rodent models (36). Previous research demonstrated that knocking out (KO) PMP22 in mice led to disrupted cholesterol distribution, abnormal lipid raft structure, and reduced capacity for ATP binding cassette subfamily A1 (ABCA1)-mediated cholesterol efflux (37). This indicates that PMP22 plays a role in regulating lipid metabolism and cholesterol transportation by interacting functionally with ABCA1, a protein involved in cholesterol efflux regulation. This interaction was further explored in this study

Another essential player in the field of lipid metabolism is the Kennedy pathway (cytidine 5'-diphosphocholine or CDP-pathway), responsible for synthesizing phosphatidylcholine (PC) and phosphatidylethanolamine (PE). These predominant cellular phospholipid species significantly contribute to myelin lipid composition (38). Substrates from the pathway (ethanolamine and choline chloride) were administered to CMT1A iPSC-SCP to assess potential positive effects on the expression of SC differentiation markers.

Lipid metabolism modulation was also tackled through stimulation of the peroxisome proliferator-activated receptor gamma (PPARγ), which regulates lipid metabolism-related gene expression (39). The effect of rosiglitazone, a PPARγ ligand, on the SC differentiation marker expression levels was examined. This was also investigated using lipid metabolism modulator LEI110, an inhibitor of PLAAT3. Under normal conditions, PLAAT3 facilitates N-acyltransferase activity, phospholipase A1 (PLA1), and PLA2, causing hydrolyzation of PC and PE at specific ester bonds, generating free fatty acids. By inhibiting PLAAT3, phospholipids can be remodeled, and the synthesis of bioactive lipids is inhibited (40). Lastly, lipid metabolism was modulated through the inhibition of SCD1, a catalyst that actively supports the synthesis of monounsaturated fatty acids (MUFA) (41).

Current therapies – A few clinical trials studied potential therapeutic approaches for CMT1A with moderate results. Hence, there are no effective CMT1A treatments available, largely because current rodent models do not fully recapitulate the human pathology. At present, patients rely on symptomatic and supportive care through surgical corrections and physical therapy (42). Those existing treatments focus on symptom management rather than the underlying pathology (18). This therapeutic gap arises from the extensive genetic landscape and clinical heterogeneity associated with CMT, underscoring the need for a more profound understanding of its molecular basis (5). The limited understanding of the disease etiology makes it challenging to create accurate disease models, hindering progress in developing targeted treatments. Because of ethical and logistical limitations, *in vitro* models of human SC are rarely used in CMT1A research. To address these challenges, patient-derived induced pluripotent stem cell (iPSC) differentiation has been introduced to generate human SC-like cells that have a high level of translatability.

Human patient-derived iPSC – Bridging this crucial gap in knowledge, this study utilized human CMT1A patient-derived iPSC and their TALEN-corrected isogenic (ISO) control, both sharing the same genetic background. This approach minimizes genetic variability and facilitates the genotype-phenotype correlation (43). Implementing iPSC as a model for CMT1A through patient-specific cell lines can rectify ethical issues. These iPSC were differentiated into SC precursor- and SC-like cells, providing a highly relevant human model to investigate the developmental metabolism abnormalities characterizing the disease. This approach helps to enhance the understanding of CMT1A pathogenesis and facilitates the identification of potential therapeutic targets by unraveling the specific mechanisms contributing to SC dysfunction (24).

Importance of this study – This study aimed to elucidate lipid metabolism disturbances and impaired differentiation by using a human CMT1A patient-derived iPSC Schwann cell model. This thesis addresses the effects of ABCA1 inhibition, lipid metabolism modulation, and purification of SCP. The primary goal was to clarify the impairments in lipid metabolism during the differentiation of CMT1A SC. Insights from this research could enhance the understanding of the pathophysiology, SC differentiation, and lipid metabolism homeostasis in CMT1A, which are all potential targets for therapeutic approaches. Ultimately, this can pave the way for developing a therapy for CMT1A.

EXPERIMENTAL PROCEDURES

iPSC-SCP cell culture – The human CMT1A patient-derived iPSC line 67i, along with its transcription activator-like effector nucleases (TALEN) corrected isogenic (ISO) control, were generously provided by Dr. Robert H. Baloh (Center for Neural Science and Medicine, Los Angeles, USA). The differentiation of iPSC into Schwann cell precursors (iPSC-SCP) was conducted at the laboratory of our collaborator Prof. Dr. Ludo Van Den Bosch at VIB-KULeuven. iPSC-SCP were cultured in Matrigel®-coated (Corning, New York, USA) culture flasks using a custom iPSC-SCP medium composed of a 1:1 mixture of DMEM-F12 (ThermoFisher Scientific, Massachusetts, USA) and Neurobasal medium (ThermoFisher). This medium was supplemented with 1% BSA-solution (Biowest, Nuaillé, France), 2mM GlutaMAX™ (ThermoFisher), 100 U/ml Penicillin & streptomycin (Pen/Strep, ThermoFisher), 1x N2 supplement (ThermoFisher), 1x B27 supplement without vitamin A (ThermoFisher), 20 µM SB (Stemcell Technologies, Vancouver, Canada), 3mM Chir (Stemcell Technologies), 0.11 mM β-mercaptoethanol (ThermoFisher), and 25 ng/ml Neuregulin (Immunotools, Friesoythen, Germany). The cells were maintained in a humidified incubator at 37°C with 5% CO_2, and the medium was refreshed every two days. Upon reaching ±80-90% confluency, the cells were detached using accutase (ThermoFisher) and harvested for subsequent experiments.

Differentiation towards iPSC-iSC – The medium and cell plate coating was changed to induce iPSC-iSC differentiation. Cells were seeded in 6-well plates (300 000/well) coated with poly-L-ornithine (PLO, 100 µg/ml, Sigma-Aldrich, Missouri, USA) and laminin (5 µg/ml) (Sigma-Aldrich) in Schwann cell precursor differentiation medium (SCPDM). The next day, SCPDM was switched to iPSC-iSC induction medium, composed of DMEM-F12 (ThermoFisher) supplemented with 100 U/ml Pen/Strep (ThermoFisher), 40 µM SB (Stemcell Technologies), 6 µM Chir (Stemcell Technologies), 200 nM Retinoic acid (ThermoFisher), 20 ng/ml PDGF-bb (Immunotools) 5 µM Forskolin (Stemcell technologies), and 200 ng/ml NRG1 type III (Immunotools). Two days later, the medium was changed to iPSC-iSC differentiation medium, composed of DMEM-F12 (ThermoFisher) supplemented with 100 U/ml Pen/Strep (ThermoFisher), 0.005% BSA (Biowest), 20 µM SB (Stemcell technologies), 3 µM Chir (Stemcell technologies), 100 nM Retinoic acid (TermoFisher Scientific), 10 ng/ml PDGF-bb (Imunotools), 5 µM Forskolin (Stemcell Technologies), and 200 ng/ml NRG1 type III (Immunotools). Two days later, the medium was again changed to iPSC-iSC final medium, composed of DMEM-F12 (ThermoFisher) supplemented with 100 U/ml Pen/Strep (ThermoFisher), 0.005% BSA (Biowest), 5 µM Forskolin (Stemcell Technologies), and 200 ng/ml NRG1 type III (Immunotools) (Supplementary Fig. 1). After two days, iPSC-iSC cell lysates were collected in Qiazol (Qiagen, Hilden, Germany) and stored at -80°C until further usage.

Lipid metabolism modulation – Lipid metabolism modulation was performed using iPSC-SCP and iPSC-iSC. Rosiglitazone (PPARγ-agonist; 1 µM, MedChemExpress, New Jersey, USA), PSC-833 (ABCA1-inhibitor; 1 µM; Tocris Bioscience, Bristol, UK), ethanolamine (Kennedy pathway substrate; 1 mM; ThermoFisher), choline chloride (Kennedy pathway substrate; 1 mM; ThermoFisher), CAY10566 (SCD1 inhibitor; 300 nM; MedChemExpress), glucosylceramide (Kennedy pathway stimulator; 200 µM; Sigma-Aldrich, Missouri, USA), cholesterol (50 µM), oleic acid (18:1, 50 µM) was administered, prepared in PBS (ThermoFisher) or DMSO (ThermoFisher) that served as controls. Final working solutions were added to the cell culture medium (1/100) to reach the previously mentioned concentrations.

Immunocytochemistry (ICC) – Initially, cells were fixed using 4% paraformaldehyde (PFA, Sigma-Aldrich) in PBS for 15 minutes, followed by permeabilization using 0.05% Tween 20 (Sigma-Aldrich). Subsequently, the cells were rinsed with PBS and blocked using a 10% blocking solution (Dako, Santa Clara, USA). Primary antibodies (Supplementary Table 3A) were used at the specified concentrations and incubated overnight at 4°C while gently shaking. Next, secondary antibodies (Supplementary Table 3B) were added at a 1/300 dilution in blocking buffer and incubated for 2 hours at room temperature (RT) in the dark while gently shaking. Nuclei were stained with DAPI (1/10 000, ThermoFisher) for 10 minutes at RT. Finally, the cells were mounted using Shandon Immunomount™ (ThermoFisher). Images were generated using the Leica DM400 B LED fluorescence microscope (Leica, Diegem,

Belgium) equipped with the Leica Application Suite X software and analyzed using the ImageJ software version 2.3.0 (Fiji, Maryland, USA). Unbiased integrated density was calculated using a self-made ImageJ script.

RNA isolation and cDNA synthesis – Qiazol lysates were thawed on ice, 100 µL of chloroform was added, and samples were resuspended, followed by an incubation period of 2-5 minutes until phase contrast was visible. Next, samples were centrifuged at 14 000 rpm for 15 minutes at 4°C. Then, 200 µl of the aqueous phase was pipetted into a new tube containing 2 µl glycogen, after which 200 µl 2-isopropanol was added, and the mixture was thoroughly mixed by agitation. Samples were dried for 30 minutes at RT, then centrifuged at 14,000 rpm for 10 minutes at 4°C. The supernatant of the pellet was removed, and 800 µl cold (4°C) 75% ethanol was added to the cell pellet, followed by 10-minute centrifugation for washing the sample. Finally, the pellet was completely dried for further use to check the amount of RNA with the NanoDrop.

Quantitative PCR – A qPCR mastermix was prepared, containing SYBR green (Applied Biosystems, Massachusetts, USA), and targeted primers (Supplementary Table 4). Subsequently, 7.5 µl of the qPCR mastermix was mixed with 2.5 µl of cDNA samples, with Milli-Q blanks serving as negative controls. After a brief centrifugation step at 1200 rpm, the qPCR reaction was initiated using the QuantStudio 3 RT-PCR system (Thermo Fisher Scientific, Massachusetts, USA), initiating with a holding stage at 95°C for 20 seconds, followed by a cycling stage at 9°C for 3 seconds and 60°C for 30 seconds, repeated for 40 cycles. A melt curve stage ensued at 95°C for 15 seconds, 60° for 1 minute, and 95°C for 15 seconds. The samples were analyzed using the QuantStudio software. Housekeeping genes RPL13A and YWHAZ served as internal controls for analyzing qPCR data.

Generalized Polarization analysis – iPSC-SCP were labeled with a Nile red dye (ThermoFisher). Spectral imaging was performed using the LSM880 NLO AiryScan microscope (Zeiss, Jena, Germany). Generalized polarization (GP) values, ranging from -1 to +1 for spectral analysis with Nile red, were calculated using an ImageJ GP plug-in based on the obtained emission wavelengths (Supplementary Methods).

Magnetic-activated cell sorting (MACS) – MACS-buffer was prepared by combining phosphate-buffered saline (PBS), pH 7.2, 0.5% bovine serum albumin (BSA), and 2mM EDTA which was subsequently stored at -20°C. Cells were harvested and dissociated to a single-cell suspension by passing through a 30 µm nylon mesh. After removing the supernatant, the cell pellet was resuspended in MACS buffer. Neural Crest Stem Cell MicroBeads (anti-CD271 or p75NGFR; Miltenyi Biotec, Cologne, Germany) were added, and the mixture was incubated at 4°C for 15 minutes. Before using the MS columns (Miltenyi Biotec), they were rinsed with MACS buffer.

For isolation of Schwann cells (p75NGFR-positive fraction), cells were washed with 2ml of MACS buffer and centrifuged, and the cell pellet was resuspended in 500µl MACS buffer. Magnetic separation was performed using MS columns and a MACS separator (Miltenyi Biotec). The cell suspension was applied to the MS columns to isolate undifferentiated cells (p75NGFR-negative fraction), and the flow-through containing unlabeled cells was collected. The positive isolation containing the labeled Schwann cells was obtained by removing the MS column from the MACS separator and placing it in a new collection tube. MACS buffer was added and immediately flushed out by pushing a plunger to collect the positive labeled fraction. Positive and negative cell suspensions were seeded for further analysis.

Statistics – Data were checked for normality using the Shapiro-Wilk test before analysis. Data that followed a normal distribution were analyzed with either a Student's t-test (for comparisons between 2 groups) or a one-way analysis of variance (ANOVA) followed by Tukey's post hoc multiple comparison test. The Mann-Whitney U test was used for data that did not follow a normal distribution. All other statistical analyses and graphs were created using GraphPad Prism Version 10.2.0 (392) (GraphPad Software Inc, San Diego, USA). Data are presented as means ± standard deviation (SD), and significance was considered with a probability of *P<0.05, **P<0.01, ***P<0.001, and ****P<0.0001. All figures were modified and finalized in Microsoft PowerPoint (version 2022).

RESULTS

Increased expression of SC differentiation markers in iPSC-iSC compared to iPSC-SCP – First, the differentiation protocol was validated, and key changes were identified in the mRNA levels of differentiation markers between iPSC-SCP and iPSC-iSC (Fig. 2). In general, differentiation markers were increased in the iPSC-iSC compared to the iPSC-SCP, indicating the successful maturation during our differentiation protocol. Furthermore, gene expression profiles were different between CMT1A and ISO controls. Differentiation markers MPZ, SOX2, SOX10, NCAM, CJUN, CD90, and LAMA4 mRNA levels were significantly higher in ISO and CMT1A iPSC-iSC compared to ISO iPSC-SCP. Meanwhile, mRNA levels of KROX20 were not significantly altered in ISO iPSC-iSC and CMT1A iPSC-iSC compared to ISO iPSC-SCP. For the P75 NTR gene expression levels, only a significant difference between ISO iPSC-SCP and ISO iPSC-iSC was observed. Additionally, to determine the expression of SC differentiation markers on a protein level, immunofluorescence assays were performed (Fig. 3-3M). A significant decrease in *MPZ* was observed in CMT1A iPSC-SCP and ISO iPSC-iSC compared to ISO iPSC-SCP, while an increase of *MPZ* was observed in CMT1A iPSC-iSC compared to CMT1A iPSC-SCP (Fig. 3A-3a, 3G-3g). *SOX2* showed a significant increase in CMT1A iPSC-iSC compared to CMT1A iPSC-SCP (Fig. 3B-3b, 3H-3h), whilst *OCT6* protein levels were significantly increased in ISO iPSC-iSC compared to ISO iPSC-SCP (Fig. 3C-3c, 3I-3i). A significant increase in *P75 NTR* protein expression was observed in CMT1A iPSC-iSC compared to both ISO iPSC-SCP and CMT1A iPSC-SCP, and *P75 NTR* was significantly upregulated in ISO iPSC-iSC compared to ISO iPSC-SCP (Fig. 3D-3d, 3J-3j). Protein levels of *KROX20* were significantly upregulated in CMT1A iPSC-iSC compared to both ISO and CMT1A iPSC-SCP (Fig. 3E-3e, 3K-3k). Differentiation marker *CJUN* did not show significant alterations (Fig. 3F-3f, 3L-3l).

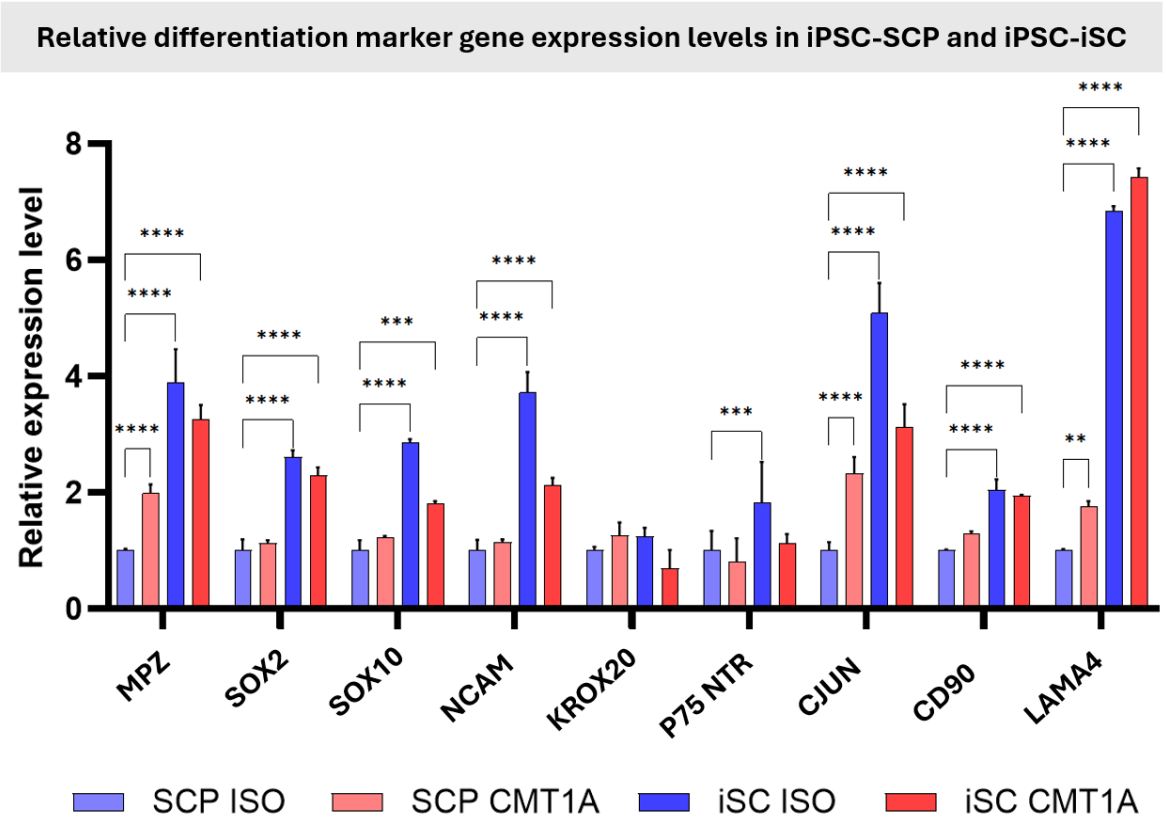

Figure 2 – Schwann cell differentiation markers are increased in iPSC-iSC compared to iPSC-SCP on an mRNA level, and are different in CMT1A compared to ISO. Relative gene expression levels in iPSC-SCP and iPSC-iSC for ISO (blue bars) and CMT1A (red bars). All groups were statistically compared to the iPSC-SCP ISO group. 1 experimental repeat. **P<0.01, ***P<0.001, ****P<0.0001. Data are presented as mean ± SD. Mann-Whitney U test.

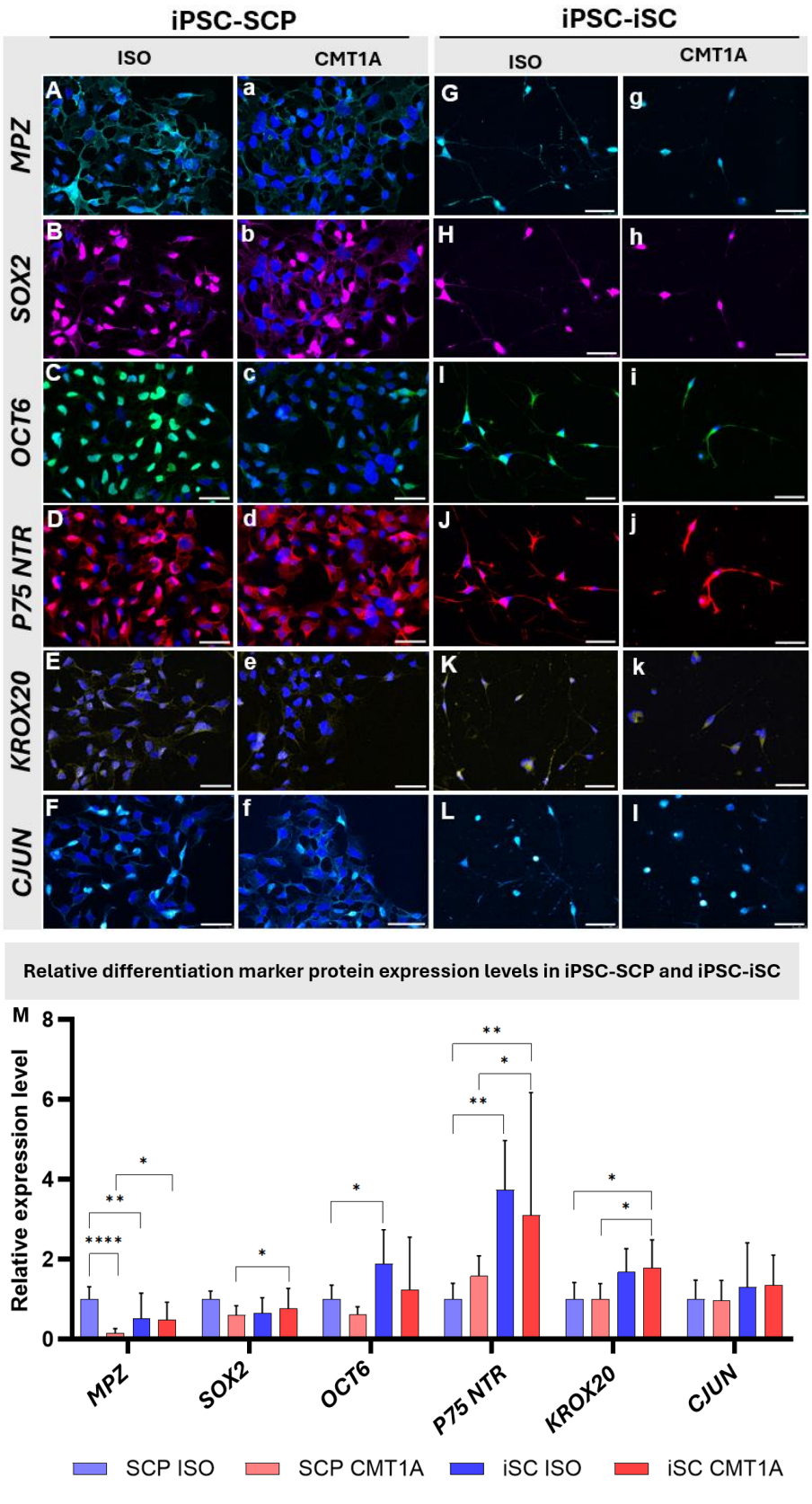

Figure 3 – Schwann cell differentiation markers are increased in iPSC-iSC compared to iPSC-SCP on a protein level. Relative protein expression of SC differentiation markers in iPSC-SCP and iPSC-iSC for ISO (3M; blue bars) and CMT1A (3M; red bars). DAPI-nuclear staining in blue. All groups were compared to ISO iPSC-SCP. 1 experimental repeat. *P<0.05, **P<0.01, ***P<0.001, ****P<0.0001. Data are presented as mean ± SD. Integrated density was normalized and compared between ISO and CMT1A iPSC-SCP and iSC. Scale bar = 50 µm, n = minimum of 477 cells/ISO SCP group and 342 cells/CMT1A SCP group, n = minimum of 60 cells/ISO iSC group and 55 cells/CMT1A iSC group. Mann-Whitney U test (M).

The cholesterol efflux regulatory protein ABCA1 is significantly upregulated in CMT1A – Bulk RNA sequencing was performed on ISO and CMT1A iPSC-iSC to understand how alterations in gene expression may translate to disturbed lipid profiles in CMT1A (32). Surprisingly, we observed that the cholesterol efflux regulatory protein, also called ATP binding

cassette subfamily A1 (ABCA1), was significantly upregulated in CMT1A (Fig. 4A). In almost all cells, cholesterol homeostasis is maintained through an ABCA1-dependent cholesterol efflux (44). Furthermore, PMP22 is known to regulate ABCA1-mediated cholesterol efflux, making this mechanism in CMT1A a potential therapeutic target. In addition, immunocytochemistry indicated an increased presence of *ABCA1* in CMT1A iPSC-SCP, confirming the RNA sequencing data (Fig. 4B-4D).

An increase in ABCA1 may lead to an excessive efflux of cholesterol, potentially disturbing cholesterol homeostasis. Therefore, ABCA1 was inhibited using PSC-833, a non-immunosuppressive cyclosporine that inhibits ABCA1-mediated cholesterol efflux (Fig. 4E). PSC-833-mediated ABCA1 inhibition significantly increased the gene expression levels of SC differentiation markers (MPZ, CJUN, CAD19, and SOX10) in CMT1A iPSC-SCP, with the highest increase observed at the 1 µM concentration. Conversely, a slight decrease was noted in the expression of LAMA4 and SOX2 in CMT1A iPSC-SCP (Fig. 4F). These findings were confirmed using immunocytochemistry for *MPZ* on CMT1A iPSC-SCP (Fig. 4G-4J), as *MPZ* was significantly higher in CMT1A after supplementation of 1 µM and 2.5 µM PSC-833 (Fig. 4K).

Generalized polarization analysis using Nile Red revealed a difference in CMT1A lipid membrane order **–** Membrane ordering was studied by calculating General Polarization (GP)-values using Nile Red. Nile Red is a fluorescent probe that stains neutral lipid droplets, allowing the measurement of total lipid content and the characterization of the organization of membranes. To characterize the spectral shift, the GP method is an established assay based on measuring the intensity in two different spectral windows at shorter and longer wavelengths within the emission spectrum of the probe (45). GP-values range from -1 to +1, indicating more or less membrane disorder, respectively. Spectral analysis revealed an altered lipid order and packing in CMT1A iPSC-SCP. Since cholesterol homeostasis is known to be disturbed in CMT1A SC, cells were supplemented with either cholesterol (Fig. 5A-5a), a combination of cholesterol and oleic acid (OA) (Fig. 5B-5b), or OA alone (Fig. 5C-5c). OA is the most common monounsaturated fatty acid in the human diet, and it is known to stimulate lipid droplet formation when given in overload to eukaryotic cells (46). After 24h of supplementation, cells were stained with Nile Red and whole cell GP-values were calculated, and ISO and CMT1A iPSC-SCP were compared (Fig. 5D). Cholesterol exposure resulted in a more fluid or disordered membrane state (GP = ± -0.8), while OA treatment improved membrane order in all conditions (GP = ± -0.4) (Fig. 5D). Exposure of ISO and CMT1A iPSC-SCP to the combination of cholesterol and OA indicated a significant difference between CMT1A and ISO cells. CMT1A iPSC-SCP had a mean GP-value of -0.3, while ISO iPSC-SCP showed a GP-value of -0.65 (Fig. 5D). This indicates a less disordered membrane composition after the combined treatment in CMT1A. A 5-day treatment with OA or cholesterol showed increased gene expression of all SC differentiation markers in iPSC-SCP, reaching significance for MBP and KROX20 (Fig. 5E). In general, these findings indicate a general disturbance in the CMT1A lipid membrane order.

Kennedy pathway substrates improve the expression of SC differentiation markers in isogenic iPSC-iSC – Since phospholipids are the predominant cellular lipid species in SC, substrates of the Kennedy pathway responsible for *de novo* phospholipid synthesis were supplemented to ISO and CMT1A iPSC during their differentiation to iSC. The Kennedy pathway consists of two branches, in which choline and ethanolamine each act as a substrate of their respective branch. This results in the end production of phosphatidylcholine (PC) and phosphatidylethanolamine (PE), respectively (Fig. 6A). Choline and ethanolamine both significantly increased the gene expression of all SC differentiation markers in ISO iPSC-SCP. Surprisingly, these Kennedy pathway substrates had minimal effect on gene expression levels in differentiating CMT1A iPSC-SCP (Fig. 6B).

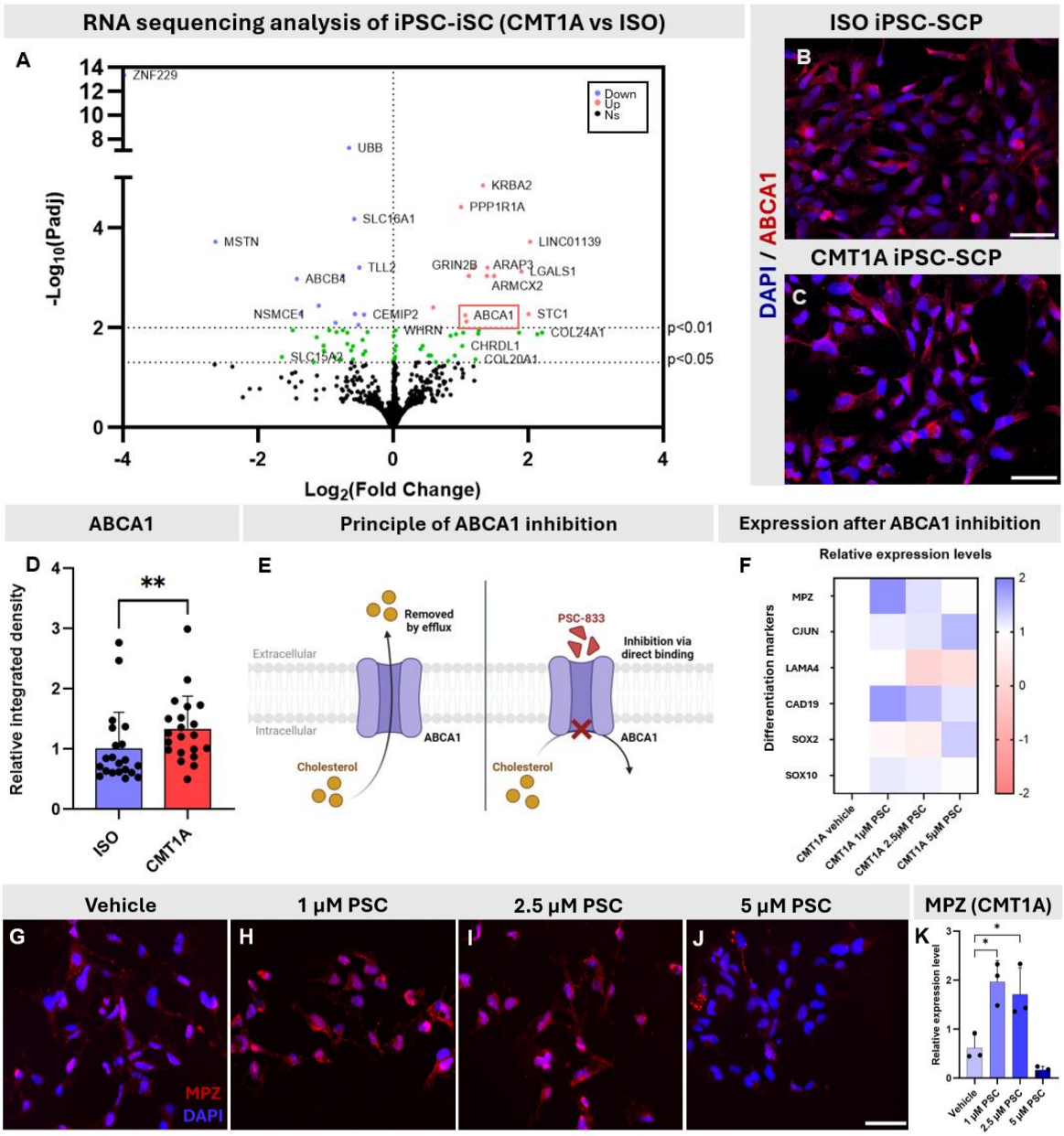

Figure 4 – ABCA1 is significantly upregulated in CMT1A. (A) Volcano plot of RNA sequencing showing relative expression profiles in CMT1A iPSC-iSC. Red/purple defines up/downregulation according to adjusted P-values. The P-value threshold was set at 0.05 and 0.01. ABCA1 is highlighted with a red square. (B-C) Representative images of ABCA1 immunocytochemistry in ISO iPSC-SCP (B) and CMT1A iPSC-SCP (C). n = minimum of 1240 cells for ISO and 1047 cells for CMT1A. (D) Relative integrated density was measured, normalized, and compared between ISO iPSC-SCP and CMT1A iPSC-SCP. (E) Illustration of ABCA1-mediated cholesterol efflux mechanism and principle of ABCA1 inhibition using PSC-833. (F) Heatmap illustrating the mean relative expression levels of SC differentiation markers in CMT1A iPSC-SCP across concentrations of PSC-833 (vehicle, 1 µM, 2.5 µM, 5 µM). (G-J) Representative images of MPZ immunocytochemistry after PSC-833 exposure in CMT1A iPSC-SCP. (K) Relative integrated density was normalized, and compared with vehicle control. From n = 1 patient. Scale bar = 50 µm. *P<0.05, **P<0.01. Data are presented as mean ± SD. Unpaired two-tailed t-test (D) or Mann-Whitney U test (K). DAPI nuclear staining in blue.

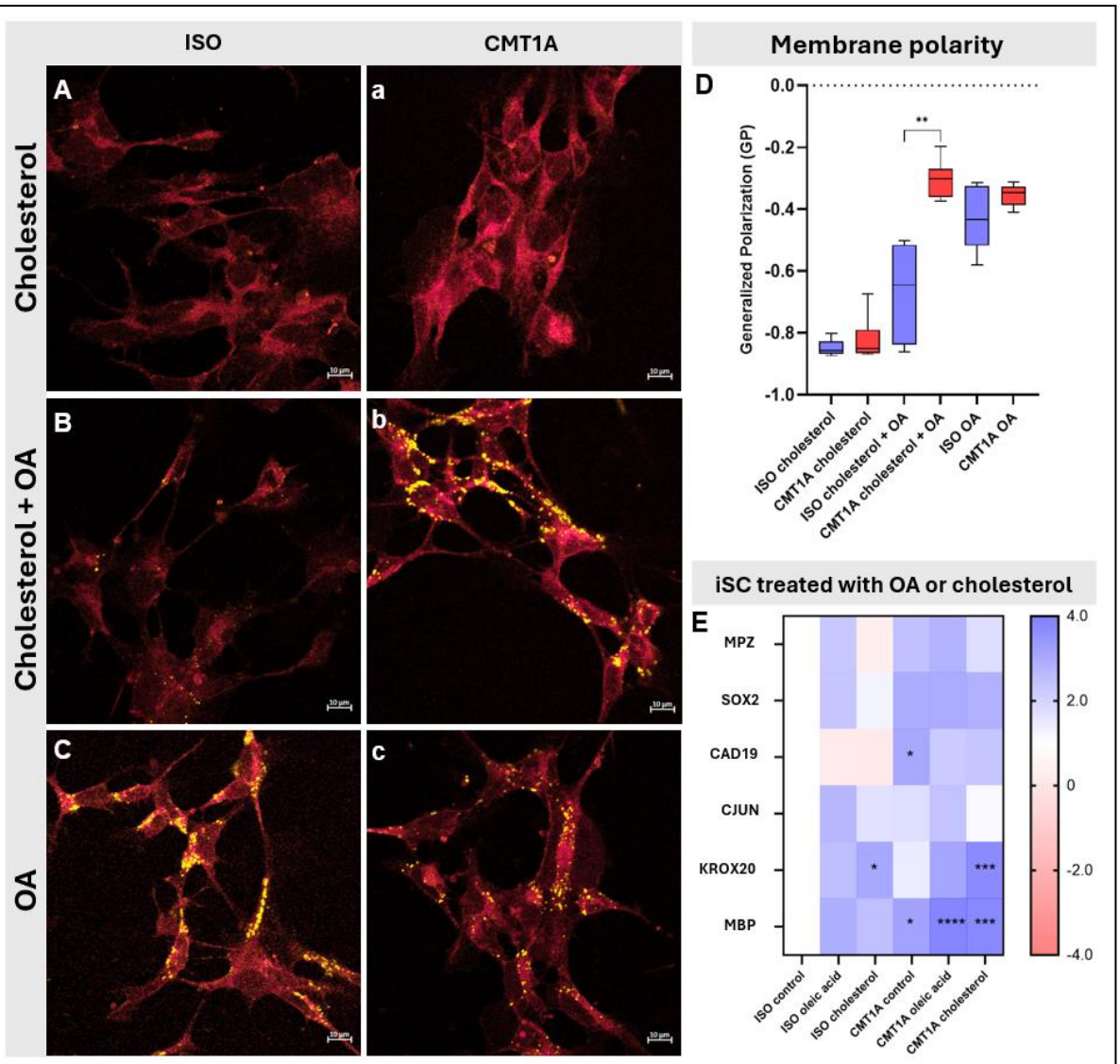

Figure 5 – Generalized polarization analysis using Nile Red revealed a difference in membrane lipid membrane order in CMT1A after the combined administration of cholesterol and oleic acid. (A) Representative images of Nile Red staining in CMT1A (a-c) and ISO (A-C) SCP treated with cholesterol (50 µM), oleic acid (50 µM), or the combination of cholesterol and OA. (D) Generalized Polarization (GP)-values were calculated from the fluorescence emission intensity at two different wavelengths (red and blue) using an Image-J plug-in. GP-values were normalized and compared between ISO and CMT1A. (E) Heatmap of the gene expression of SC differentiation markers in SCP after addition of OA or cholesterol. N=1; Scale bars: 10 µm, 1 experimental repeat. *P<0.05, **P<0.01, ***P<0.001, ****P<0.0001. Data are presented as mean ± SD. Unpaired two-tailed t-test (D) or Mann-Whitney U test (E).

Lipid metabolism-modulation in (differentiating) SCP can alter SC differentiation marker gene expression levels – After observing a perturbed lipid metabolism in CMT1A cells, we aimed to activate the lipid-regulating PPARγ pathway using rosiglitazone in iPSC-SCP for 3 days (Fig. 6C). Overall, this resulted in an increased gene expression of SC differentiation markers in ISO iPSC-SCP (MPZ, SOX2, SOX10, CAD19, MBP, CJUN, KROX20, CD90, and LAMA4). In CMT1A iPSC-SCP, rosiglitazone treatment did not induce an increase in all markers, however, we observed an increased expression of MPZ, SOX10, CAD19, MBP, CJUN, and LAMA4.

Additionally, we stimulated the Kennedy pathway in iPSC-SCP using glucosylceramide (GluCer) for 3 days. In CMT1A iPSC-SCP, GluCer increased the expression of MPZ, SOX2, SOX10, CJUN, KROX20, CD90, and LAMA4 (Fig. 6C).

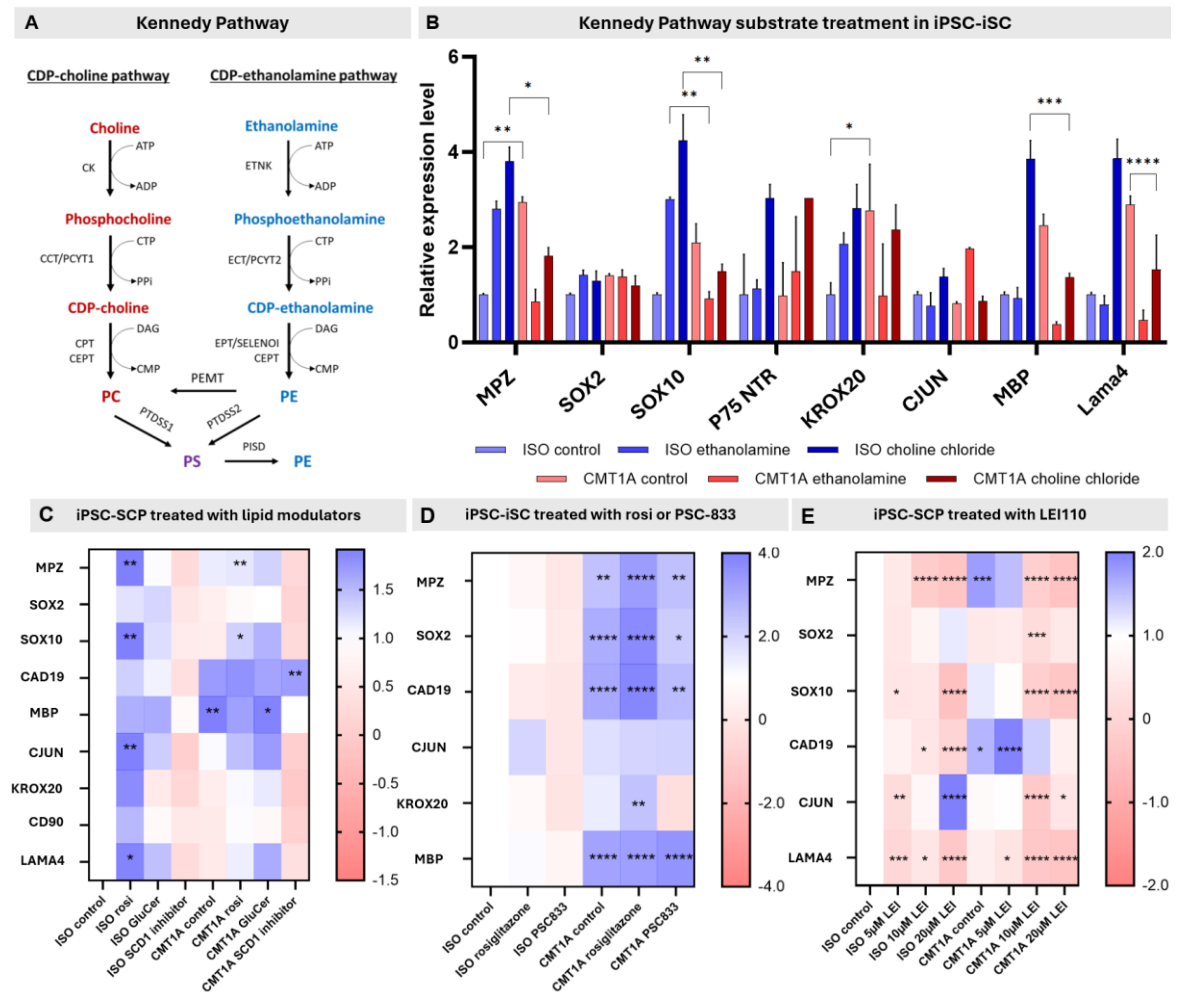

Figure 6 – Supplementation of Kennedy Pathway substrates improves the gene expression of SC differentiation markers in ISO iSC. (A) Illustration of the Kennedy Pathway (KP), which consists of 2 branches – CDP-choline and CDP-ethanolamine – that lead to the end production of phosphatidylcholine (PC) and phosphatidylethanolamine (PE). (B) Relative gene expression levels of SC differentiation markers in ISO and CMT1A iPSC-iSC after adding ethanolamine or choline chloride, for 3 days. (C) ISO and CMT1A SCP were treated with rosiglitazone (rosi), glucosylceramide (GluCer), or PSC-833 for 3 days. (D) ISO and CMT1A iPSC-iSC were treated with rosiglitazone or PSC-833 for 5 days. (E) ISO and CMT1A SCP were treated with various concentrations of LEI110 (5 µM, 10 µM, 20 µM) for 24 hours. N = 1 experimental repeat. All groups were statistically compared to the ISO control group. *P<0.05, **P<0.01, ***P<0.001, ****P<0.0001. Data are presented as mean SD. Mann-Whitney U test or ANOVA followed by Tukey's post hoc multiple comparison test.

Cells were also treated for 3 days with an inhibitor of Stearoyl-CoA 9-desaturase 1 (SCD1), the rate-limiting enzyme for unsaturated fatty acid synthesis. SCD1 inhibition significantly reduced the gene expression levels of all SC differentiation markers in CMT1A iPSC-SCP, showing the importance of unsaturated fatty acids in SC differentiation (Fig. 6C).

Interestingly, a 5-day treatment with rosiglitazone significantly increased the expression of all SC differentiation markers in CMT1A iPSC-iSC, but slightly decreased the expression of these markers in ISO control iPSC-iSC (Fig. 6D). Moreover, a 5-day treatment using PSC-833 (ABCA1-inhibitor) notably increased the expression of all SC differentiation markers in CMT1A iPSC-iSC, except for KROX20. In contrast, PSC-833 decreased the expression of all markers, except CJUN in ISO iPSC-iSC (Fig. 6D).

A 24-hour lipid modulation treatment with the PLAAT3 inhibitor, LEI110, showed a dose-dependent decrease in the expression of most SC

differentiation markers in ISO (except CJUN) and CMT1A (except CAD19 and MPZ) iPSC-SCP.

Magnetic-activated cell sorting (MACS) enhances the homogeneity of iPSC-SCP cultures. – Another objective of this study was to purify the heterogeneous SCP population resulting from the differentiation protocol (Fig. 7A). By using MACS, target iPSC-SCP can be distinguished from undifferentiated cells to achieve a more uniform cell distribution. This step would enhance the interpretability of future data. MACS was performed to purify the SCP population, and separate SCP from undifferentiated cells (Fig. 7C). A clear morphological difference was present between the positive (P75-NGFR-positive; Schwann cells) and negative selection (P75-NGFR-negative; undifferentiated cells) (Fig. 7D-7F). In addition, the gene expression profiles between both populations were compared via qPCR. Here, the gene expression levels of SC differentiation markers MPZ, CJUN, LAMA4, CD90, SOX2, SOX10, NCAM, and KROX20 were significantly lower in the negative selection of ISO iPSC-SCP

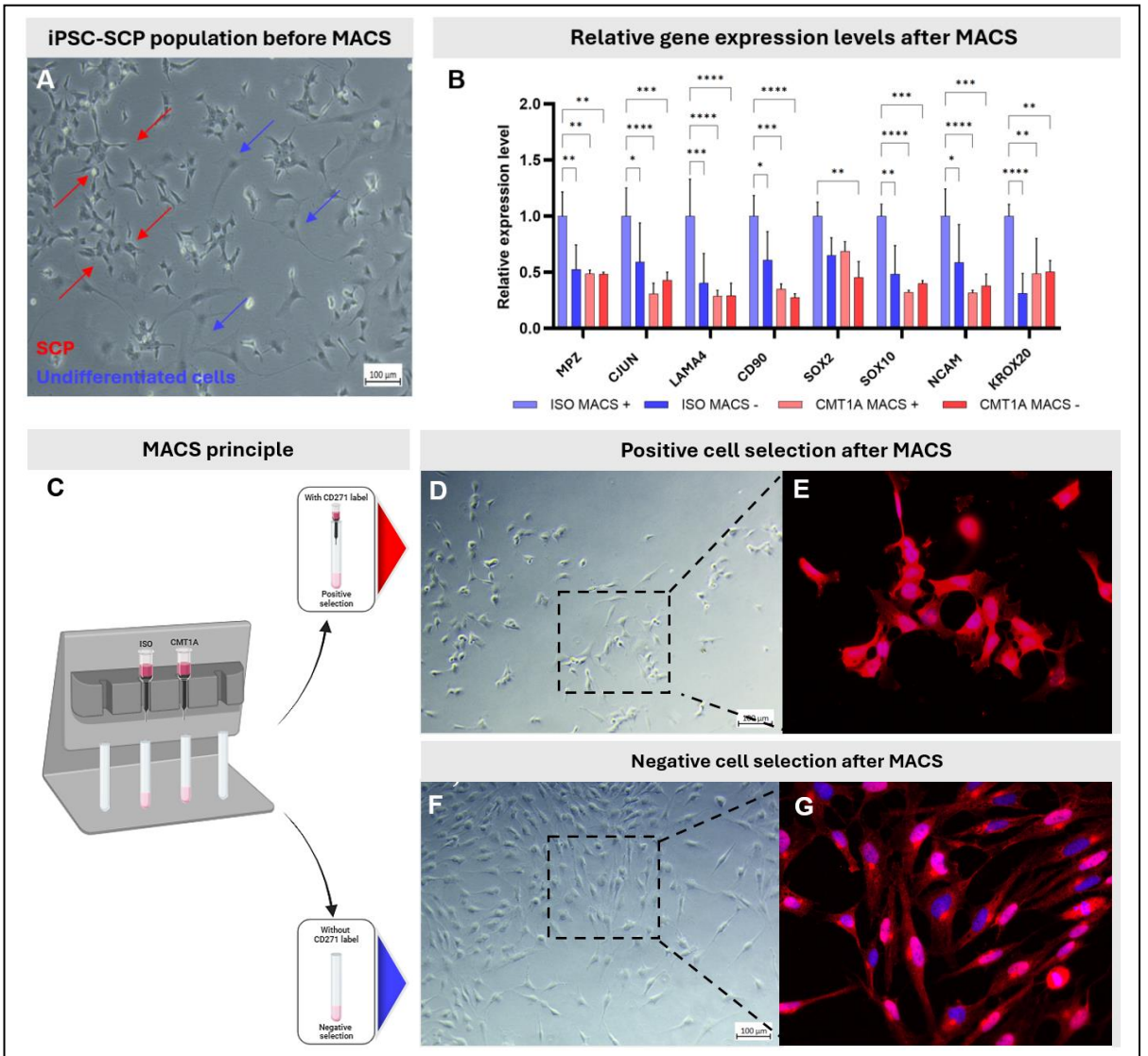

Figure 7 – MACS successfully purifies iPSC-SCP. (A) Light microscopic image of SCP before MACS. SCP (red arrows) and undifferentiated cells (blue arrows). Scale bar = 100µm. (B) Relative gene expression of SC differentiation markers in the positive and negative populations (ISO and CMT1A iPSC-SCP). (C) Illustration representing the principle of MACS. Schwann cells are characterized by a P75-NGFR-positive or CD271-positive phenotype (D-E), whereas undifferentiated cells are characterized by their P75-NGFR-negative or CD271-negative phenotype (E-G). Representative images of S100 immunocytochemical staining, combined with DAPI-counterstaining. N = 1 experimental repeat. *P<0.05, **P<0.01, ***P<0.001, ****P<0.0001. Data are presented as mean ± SD. Mann-Whitney U test.

(Fig. 7B). Besides, the expression of the SC marker S100 was analyzed via immunofluorescence on both populations. Remarkably, S100 was expressed in both populations. Nevertheless, the intensity of S100 was significantly increased in the positive selection, representing the SCP (Fig. 7E-7G; quantification not shown).

DISCUSSION.

The aim of this study was to investigate the impact of lipid metabolism modulation on the differentiation of human CMT1A iPSC-SC to unveil the underlying mechanisms perturbed in this process. This mainly concerned the comparison between SC differentiation markers in iPSC-SCP and iPSC-iSC, modulation of cholesterol metabolism in iPSC-SCP, and modulation through multiple other lipid modulators in both iPSC-SCP and iPSC-iSC. Additionally, MACS was performed and optimized in order to purify the iPSC-SCP population and separate them from undifferentiated cells.

Previous studies have provided evidence for disturbances in Schwann cell lipid metabolism (32, 34, 36). Nevertheless, human *in vitro* research in lipid metabolism modulation regarding SC differentiation was lacking and was therefore examined in this research.

This study explored the differential gene and protein expression between iPSC-SCP and iPSC-iSC of SC differentiation markers. SC are pivotal players in PNS development, myelination, providing axons metabolic support, and nerve repair responses. Understanding their differentiation process is crucial for harnessing their potential in therapeutic applications.

One key distinction between SCP and iSC lies in their differentiation state. This contrast is reflected in the differential expression patterns of specific SC markers associated with distinct developmental stages (47). Genetic expression is regulated at various levels, and differences between iPSC-SCP and iPSC-iSC can affect gene and protein expression (48). iPSC-SCP interact more with their microenvironment, influencing their expression profiles, while iPSC-iSC have less intracellular communication, leading to different expression dynamics (49). Furthermore, the detection techniques' sensitivity can introduce variability, complicating comparative analyses between iPSC-SCP and iPSC-iSC (50).

The expression levels of $P75^{NTR}$, one of the most widely used SC markers, were significantly increased in gene and protein levels in iPSC-iSC. The transcription factors SOX2, SOX10, OCT6, and KROX20 regulate SC development, differentiation, and myelination. We found that SOX2 and SOX10 showed similar gene expression levels in ISO and CMT1A iPSC-SCP and iPSC-iSC, while KROX20 showed differential expression patterns on both levels. *OCT6* was analyzed on a protein level and showed differential expression in ISO iPSC-iSC compared to ISO iPSC-SCP. *OCT6* regulates myelination via the downstream transcription factor *KROX20*, thereby affecting *MPZ* expression in more mature SC (51). We observed a significant increase in MPZ gene expression in CMT1A iPSC-SCP and CMT1A iPSC-iSC compared to ISO iPSC-SCP, while a decrease in *MPZ* protein levels was seen in CMT1A iPSC-SCP compared to ISO iPSC-SCP and CMT1A iPSC-iSC. NCAM is an *in vivo* marker of iPSC-iSC and non-myelinating SC and was significantly upregulated in ISO and CMT1A iPSC-iSC compared to ISO iPSC-SCP (31). CJUN is known to be activated in the SC of injured nerves and controls the conversion of myelinating SC into a repair type of cell (52). CMT1A iPSC-SCP showed significantly increased CJUN mRNA levels, suggesting a potential shift to a dedifferentiated SC phenotype, similar to repair SC after nerve injury. In contrast, a decrease in CJUN mRNA levels was observed in CMT1A iPSC-iSC. No significant differences in *CJUN* protein expression were observed. Fibroblast marker CD90 was included to check the degree of heterogeneity and differentiation state. Quantification of CD90 gene expression revealed that CD90-positive cells were significantly more present in the ISO and CMT1A iPSC-iSC population compared to the iPSC-SCP population, which is not arbitrary since iSC are in a more mature differentiation state. Lastly, since iSC start developing a basal lamina that contains multiple laminins that have specific functions, LAMA4 (laminin-411) was analyzed (53). Our findings suggested a significant increase in LAMA4 in both ISO and CMT1A iPSC-iSC, which was expected as basal lamina starts developing in this differentiation state, indicating a successful differentiation towards iSC.

In conclusion, both ISO and CMT1A iPSC-iSC showed significantly higher gene and protein expression levels of all examined SC differentiation markers compared to iPSC-SCP. These findings align with previous *in vivo* and *in*

vitro studies (31, 54). Of note, earlier research showed that *in vivo* iSC do not express *Krox20*, suggesting that *in vitro* cultured iPSC-iSC are similar, but not identical to *in vivo* iSC (31). This underscores the need for more translatable models, such as the patient-derived human iPSC-SCP model used in our study. However, recent studies have shown evidence that iPSC-SCP are highly multipotent, reflecting the diverse roles of SCP beyond PNS development and making them very similar to neural crest cells. This may limit the accuracy of the iPSC-SCP model for certain interpretations (55). Despite these limitations, the evidence supports the use of this iPSC-SCP model for CMT1A research, making it currently preferable to other *in vitro* CMT1A models, excluding the *PMP22*-overexpressing dental pulp stem cells (DPSC), which are also studied in our lab (56). Ideally, future research should aim to integrate the advantages of human-derived iPSC and DPSC to address the limitations of each CMT1A SC model. This could involve the development of a 3D peripheral nerve-like environment to create a more robust human CMT1A *in vitro* model, but further research is needed.

Furthermore, previous research has identified cholesterol biosynthesis as one of the main canonical pathways that are downregulated in sciatic nerves of CMT1A mouse models (36). Bulk RNA sequencing data of iPSC-iSC and immunofluorescence data of iPSC-SCP both confirmed significant upregulation of ABCA1 in CMT1A cells. Since ABCA1 regulates cholesterol and phospholipid efflux by transporting it to lipid-poor apolipoproteins (ApoA), ABCA1 upregulation could be involved in the process of impaired cholesterol homeostasis in CMT1A SC (57). An upregulated ABCA1 expression, means more cholesterol efflux, thereby reducing intracellular cholesterol levels and possibly altering the membrane composition. Besides, high cholesterol levels are crucial for the stability and compactness of the myelin sheaths (58). An imbalance due to increased efflux might influence the myelination process or maintenance of existing myelin. Moreover, cholesterol-rich domains in the membrane, known as lipid rafts, are important for the function of myelin proteins. Altered cholesterol levels might affect their localization and function, resulting in altered regulation of membrane receptor signaling and myelination (36). Moreover, a study by *Zhou et al.* revealed that the perturbed molecular mechanisms behind cholesterol trafficking and lipid homeostasis in CMT1A SC involve a functional interplay among PMP22, cholesterol, ApoA-E, and ABCA1 (37).

Therefore, as a next step in our study, we blocked the activity of ABCA1 by adding PSC-833 to isogenic and CMT1A iPSC-SCP and iPSC-iSC to prevent cholesterol efflux. Previously, it has been shown that PSC-833 causes an effective inhibition via direct binding of P-glycoproteins, the most extensively studied ATP-binding cassette (ATP) transporters, including ABCA1 (59). Interestingly, our findings showed increased mRNA and protein expression levels of SC differentiation markers after ABCA1 inhibition. Since cholesterol efflux was inhibited, more intracellular cholesterol accumulation can beneficially affect signaling pathways, critical for SC differentiation, through altered composition and organization of lipid rafts. Moreover, ABCA1 is regulated by liver X receptors (LXR), nuclear receptors sensitive to cholesterol levels. The inhibition of ABCA1 might lead to altered LXR activity, impacting the expression of genes involved in lipid metabolism and differentiation (60). High concentrations of PSC-833 appeared toxic for the iPSC-SCP population. Given the IC_{50} of PSC-833 (1.9 µM), this is not arbitrary (59). However, further research is needed to fully understand the implications of ABCA1 inhibition on SC differentiation marker expression levels and possible effective treatment options.

Since cholesterol and other lipids are stored in cells via specialized organelles called lipid droplets (LD), cell membrane lipid properties in isogenic and CMT1A iPSC-SCP using a Nile Red probe were explored via spectral microscopic analysis. Nile Red is a fluorescent dye used for studying lipids because it changes its fluorescence characteristics based on the environment it is in (61). The GP-values after cholesterol or OA supplementation showed no significant differences in membrane polarity between isogenic and CMT1A iPSC-SCP. However, after a 24-hour combined supplementation of cholesterol and OA, the GP-value was significantly higher in CMT1A iPSC-SCP. This suggests that the membranes of CMT1A iPSC-SCP are in a less liquid-disordered phase after combined supplementation. Several factors related to lipid metabolism and the pathological mechanisms of CMT1A can explain this. These factors include altered lipid composition, custom processing of lipid metabolism pathways, abnormal membrane

protein interactions, increased oxidative stress, or imbalanced cholesterol levels in CMT1A cells.

The ability to process and store lipids is disrupted in CMT1A iPSC-SCP, resulting in an accumulation of LD when exposed to excess levels of cholesterol and OA. In response to the combined supplementation of cholesterol and OA in CMT1A iPSC-SCP, findings show abnormal lipid storage. This contrasts with previous observations made in giant plasma membrane vesicles (GPMV) from iPSC-SCP (without supplementation), using Di-4-ANEPPDHQ or Laurdan labeling. These alternative labeling strategies would be interesting to explore in the future with cholesterol and OA supplementation on the cultures used in this study since the fluorescence emission maximum, intensity, polarization, and lifetime of Nile Red vary with the cholesterol content of the membrane (36). Interestingly, Nile red exhibits significant red edge excitation shift (REES) in the presence of cholesterol, meaning that Nile Red shows a shift in its excitation wavelength towards the red end of the spectrum when cholesterol is present. This suggests that Nile Red is located in a part of the cell membrane where its movement is limited, likely due to the presence of cholesterol (61).

The GP analysis was performed on a whole cell level, making it incorrect to form bold statements since this includes diverse lipid environments (i.e. organelle membranes vs plasma membrane), which can complicate data interpretation. An LD-focused analysis could provide more specific and interpretable GP-values on lipid storage and metabolism within LD (62). Taken together, the hydrophobic fluorescent probe Nile Red is already depending on the cholesterol content of the membrane, potentially biasing result interpretation.

Since phospholipids play a crucial role (40% of lipids) in PNS myelin, cells were supplemented with Kennedy pathway substrates that increase the synthesis of phospholipids PC and PE, both key components of cellular membranes. Kennedy pathway substrate supplementation to iPSC-SCP showed increased SC differentiation marker mRNA levels in the isogenic group but not in the CMT1A group, suggesting alternative processing of these substrates in the CMT1A condition. The underlying pathology of CMT1A may interfere with the beneficial effects of the supplementation, as observed in the isogenic group. The overexpression of PMP22 in CMT1A is a genetic abnormality that may cause intrinsic cellular dysfunctions that are not easily corrected by simply supplementing the phospholipid synthesis pathway. Additionally, the ability of cells to effectively utilize the supplemented substrates may result in ineffective or incomplete activation of the pathway due to unknown reasons.

Previous research has shown that lipid trafficking and distribution in CMT1A SC are perturbed due to errors in multiple pathways, including endoplasmic reticulum (ER) stress (37). In CMT1A mouse models, ER stress activates the unfolded protein response (UPR), which can interfere with normal cellular processes such as SC differentiation (63). In CMT1A iPSC-SCP, ER stress responses may outweigh the positive effects of substrate supplementation. Additionally, even with increased synthesis of PC and PE, CMT1A iPSC-SCP may still face membrane integrity problems due to the misregulation of other crucial components, preventing the cells from fully benefiting from the supplementation. Further research is needed to understand how the Kennedy pathway could be harnessed to have an effect on the CMT1A phenotype.

In addition, iPSC-SCP were treated with other lipid modulators to look at different lipid processes that might be disrupted in CMT1A. Such as the PPARγ-ligand, rosiglitazone, which stimulates the expression of genes related to lipid metabolism (39). Previous research showed that *ex vivo* and *in vivo* treatment with rosiglitazone ameliorated defects in myelination of fatty acid synthase (FASN) deficient SC (64). Our findings align with this and show significant increases in SC marker (general and differentiation) expression levels in isogenic and CMT1A iPSC-SCP and CMT1A iPSC-iSC, making rosiglitazone an interesting drug for further research. Moreover, the effect of PLAAT3 inhibitor, LEI110, on SC differentiation marker expression was investigated in ISO and CMT1A iPSC-SCP. PLAAT3 is an enzyme involved in lipid metabolism, specifically in remodeling membrane phospholipids and lipid signaling pathways (40). Findings showed that increased concentrations of LEI110 negatively impacted most SC differentiation markers. Inhibition of PLAAT3 can disrupt the balance of phospholipid species, affecting cellular membranes essential for proper functioning and differentiation. These findings hint at the importance of phospholipid remodeling via PLAAT3 in CMT1A SC.

MACS is a fast, efficient, and cost-effective fluorescence-activated cell sorting (FACS) alternative that was performed to separate human

iPSC-SCP from undifferentiated cells to achieve a more uniform cell distribution of our iPSC-SCP population. This could be achieved by the direct isolation of SCP by MACS based on the expression of the $P75^{NTR}$ receptor, which is solely expressed by SCP and not by other contaminating cells. Protein expression of the SC marker *S100* was also detected in the negative fraction after MACS. This could be due to incomplete separation or marker overlap caused by non-specific binding of the anti-*S100* antibody, which is likely not specific to particular isotypes.

This was the first time MACS was performed on iPSC-SCP, giving valuable insights into how iPSC populations can be purified. This proves that MACS is also relevant in iPSC research since it is highly selective, scalable, and adaptable for directly purifying human iPSC-SC cultures (65). However, even more cost-effective and simpler methods appear effective for purifying cell populations. Another traditional method for purifying SC is immunopanning, which involves using a solid surface coated with a specific antibody immobilized onto a cell culture plate (66, 67). The difference in cell size and adhesion properties between human Schwann cells and undifferentiated cells, which causes the undifferentiated cells to sediment and attach more quickly, has been utilized to separate them. This method is particularly beneficial in clinical applications because it does not involve the introduction of reagents or chemicals. Nevertheless, MACS and FACS are superior for purifying heavily contaminated human SC cultures by performing repeated rounds of purification (68).

Overall, this study is mostly limited because all experiments were done on iPSC-SCP or iPSC-iSC of 1 CMT1A patient line. Therefore, all experiments should be repeated on iPSC lines of multiple CMT1A patients to confirm the changes observed in this study. Furthermore, additional accurate quantification of protein expression levels should be done via Western Blot experiments. Due to differentiation protocol difficulties, not all experiments could be performed on iPSC-iSC, while this cell type has a higher translatability and could provide us more information on what goes wrong at later stages of SC development and myelination. Nevertheless, this study provided a broad overview of CMT1A SC differentiation marker expression levels in iPSC-SCP and iPSC-iSC, and lipid metabolism modulation for CMT1A. Findings from this thesis provide new evidence for differentiation and lipid disturbances in CMT1A Schwann cells. Future studies must be conducted to map out the exact lipid species intertwined with the lipid metabolism disturbances that can alleviate the dysfunctionalities as observed in CMT1A.

CONCLUSION

To conclude, this study provides evidence for an overall disturbance in lipid metabolism homeostasis in human CMT1A patient-derived iPSC-SC, and the possibility to purify this cell population when using it *in vitro*. This adds power to recent evidence of lipid metabolism disturbances observed in CMT1A. However, the lack of consistent interpretability in the results is acknowledgeable, pointing to the need for further investigation. This highlights the complexity of lipid metabolism modulation in SC differentiation and the potential challenges in translating these findings into clinical applications. Future research directions could explore additional factors influencing lipid metabolism in SC differentiation, optimize differentiation and MACS protocols, and identify specific therapeutic targets for CMT1A treatment. These future directions can pave the way for advancements in understanding and treating CMT1A SC disturbances. The findings of this research suggest that lipid modulation could be a promising avenue for therapeutic intervention in CMT1A by restoring dysfunctional SC, an essential insight for developing personalized treatment approaches.

Acknowledgments – The completion of this thesis would not have been possible without the essential contributions of several individuals and groups. I extend my gratitude to the research group of Prof. Esther Wolfs of the Cardio & Organ Systems (COS) department at the Biomedical Research Institute (BIOMED, UHasselt) and the research group of Prof. Jeroen Bogie of the Medical Biochemistry and Immunology lab (MBIL) at the Biomedical Research Institute (BIOMED, UHasselt) for their invaluable assistance, time, effort, and educational investment throughout this project. I am especially thankful to my daily supervisor, Koen Kuipers, for his guidance in academic research, his investment of time to provide highly relevant and insightful feedback, his expertise in research methods, and his trust and mentorship during this project. I would also like to thank my second examiner, Prof. Werend Boesmans, for his valuable insights during our intermediate evaluation meeting. Moreover, I would like to thank Kasper Dehaes, Hanne Jeurissen, Nathalie Dirckx, dr. Sam Vanherle and dr. Tim Vangansewinkel for their help, feedback, guidance and support. I also appreciate the continual support of my fellow students, family, and friends throughout this internship.

Author contributions – Prof. Esther Wolfs and Prof. Jeroen Bogie conceived and designed the senior internship project and theoretical framework. Koen Kuipers supervised the study. Yara Lambrechts and Koen Kuipers were involved in the daily planning of the project and conducted the research experiments with support from Hanne Jeurissen and Kasper Dehaes. Yara Lambrechts and Koen Kuipers performed the data analysis. Koen Kuipers and dr. Sam Vanherle provided reagents for the experiments. Yara Lambrechts wrote the thesis and designed the figures, with support and feedback from Koen Kuipers, Prof. Esther Wolfs, and dr. Tim Vangansewinkel. Both Prof. Esther Wolfs and dr. Tim Vangansewinkel edited and reviewed the thesis. The authors affirm no competing interest.

REFERENCES

1. Jessen KR, Mirsky R. Schwann Cell Precursors; Multipotent Glial Cells in Embryonic Nerves. Front Mol Neurosci. 2019;12:69.
2. Verghese J, Bieri PL, Gellido C, Schaumburg HH, Herskovitz S. Peripheral neuropathy in young-old and old-old patients. Muscle Nerve. 2001;24(11):1476-81.
3. Kazamel M, Boes CJ. Charcot Marie Tooth disease (CMT): historical perspectives and evolution. J Neurol. 2015;262(4):801-5.
4. Smith AG. Charcot-Marie-tooth disease. Arch Neurol. 2001;58(6):1014-6.
5. El-Abassi R, England JD, Carter GT. Charcot-Marie-Tooth disease: an overview of genotypes, phenotypes, and clinical management strategies. PM R. 2014;6(4):342-55.
6. Bird TD. Charcot-Marie-Tooth Hereditary Neuropathy Overview. In: Adam MP, Feldman J, Mirzaa GM, Pagon RA, Wallace SE, Bean LJH, et al., editors. GeneReviews((R)). Seattle (WA)1993.
7. Saporta AS, Sottile SL, Miller LJ, Feely SM, Siskind CE, Shy ME. Charcot-Marie-Tooth disease subtypes and genetic testing strategies. Ann Neurol. 2011;69(1):22-33.
8. CMTausa.org. Types of CMT Glenolden, PA 190362024 [
9. Chalk C. Charcot-Marie-Tooth Disease. Referene Module in Neuroscience and Biobehavioral Psychology. 2017.
10. Thomas FP, Saporta MA, Attarian S, Sevilla T, Sivera R, Fabrizi GM, et al. Patient-Reported Symptom Burden of Charcot-Marie-Tooth Disease Type 1A: Findings From an Observational Digital Lifestyle Study. J Clin Neuromuscul Dis. 2022;24(1):7-17.
11. Blair IP, Nash J, Gordon MJ, Nicholson GA. Prevalence and origin of de novo duplications in Charcot-Marie-Tooth disease type 1A: first report of a de novo duplication with a maternal origin. Am J Hum Genet. 1996;58(3):472-6.
12. Raeymaekers P, Timmerman V, Nelis E, Van Hul W, De Jonghe P, Martin JJ, et al. Estimation of the size of the chromosome 17p11.2 duplication in Charcot-Marie-Tooth neuropathy type 1a (CMT1a). HMSN Collaborative Research Group. J Med Genet. 1992;29(1):5-11.
13. McGrath MC. Charcot-Marie-Tooth 1A: A narrative review with clinical and anatomical perspectives. Clin Anat. 2016;29(5):547-54.
14. Hertzog N, Jacob C. Mechanisms and treatment strategies of demyelinating and dysmyelinating Charcot-Marie-Tooth disease. Neural Regen Res. 2023;18(9):1931-9.
15. Berger P, Niemann A, Suter U. Schwann cells and the pathogenesis of inherited motor and sensory neuropathies (Charcot-Marie-Tooth disease). Glia. 2006;54(4):243-57.
16. Johnson NE, Heatwole CR, Dilek N, Sowden J, Kirk CA, Shereff D, et al. Quality-of-life in Charcot-Marie-Tooth disease: the patient's perspective. Neuromuscul Disord. 2014;24(11):1018-23.
17. Wu R, Lv H, Zhang W, Wang Z, Zuo Y, Liu J, et al. Clinical and Pathological Variation of Charcot-Marie-Tooth 1A in a Large Chinese Cohort. Biomed Res Int. 2017;2017:6481367.
18. Tavasoli M, Lahire S, Reid T, Brodovsky M, McMaster CR. Genetic diseases of the Kennedy pathways for membrane synthesis. J Biol Chem. 2020;295(51):17877-86.
19. Betters E, Charney RM, Garcia-Castro MI. Early specification and development of rabbit neural crest cells. Dev Biol. 2018;444 Suppl 1(Suppl 1):S181-S92.
20. Basch ML, Bronner-Fraser M, Garcia-Castro MI. Specification of the neural crest occurs during gastrulation and requires Pax7. Nature. 2006;441(7090):218-22.
21. Nave KA, Werner HB. Myelination of the nervous system: mechanisms and functions. Annu Rev Cell Dev Biol. 2014;30:503-33.
22. Adameyko I, Lallemend F, Aquino JB, Pereira JA, Topilko P, Muller T, et al. Schwann cell precursors from nerve innervation are a cellular origin of

melanocytes in skin. Cell. 2009;139(2):366-79.
23. Jessen KR, Mirsky R. The origin and development of glial cells in peripheral nerves. Nat Rev Neurosci. 2005;6(9):671-82.
24. Mukherjee-Clavin B, Mi R, Kern B, Choi IY, Lim H, Oh Y, et al. Comparison of three congruent patient-specific cell types for the modelling of a human genetic Schwann-cell disorder. Nat Biomed Eng. 2019;3(7):571-82.
25. Feltri ML, Poitelon Y, Previtali SC. How Schwann Cells Sort Axons: New Concepts. Neuroscientist. 2016;22(3):252-65.
26. Stewart HJ, Morgan L, Jessen KR, Mirsky R. Changes in DNA synthesis rate in the Schwann cell lineage in vivo are correlated with the precursor--Schwann cell transition and myelination. Eur J Neurosci. 1993;5(9):1136-44.
27. Topilko P, Schneider-Maunoury S, Levi G, Baron-Van Evercooren A, Chennoufi AB, Seitanidou T, et al. Krox-20 controls myelination in the peripheral nervous system. Nature. 1994;371(6500):796-9.
28. Glenn TD, Talbot WS. Analysis of Gpr126 function defines distinct mechanisms controlling the initiation and maturation of myelin. Development. 2013;140(15):3167-75.
29. Cattin AL, Burden JJ, Van Emmenis L, Mackenzie FE, Hoving JJ, Garcia Calavia N, et al. Macrophage-Induced Blood Vessels Guide Schwann Cell-Mediated Regeneration of Peripheral Nerves. Cell. 2015;162(5):1127-39.
30. Stierli S, Napoli I, White IJ, Cattin AL, Monteza Cabrejos A, Garcia Calavia N, et al. The regulation of the homeostasis and regeneration of peripheral nerve is distinct from the CNS and independent of a stem cell population. Development. 2018;145(24).
31. Liu Z, Jin YQ, Chen L, Wang Y, Yang X, Cheng J, et al. Specific marker expression and cell state of Schwann cells during culture in vitro. PLoS One. 2015;10(4):e0123278.
32. Fledrich R, Abdelaal T, Rasch L, Bansal V, Schutza V, Brugger B, et al. Targeting myelin lipid metabolism as a potential therapeutic strategy in a model of CMT1A neuropathy. Nat Commun. 2018;9(1):3025.
33. Mittendorf KF, Marinko JT, Hampton CM, Ke Z, Hadziselimovic A, Schlebach JP, et al. Peripheral myelin protein 22 alters membrane architecture. Sci Adv. 2017;3(7):e1700220.
34. Visigalli D, Capodivento G, Basit A, Fernandez R, Hamid Z, Pencova B, et al. Exploiting Sphingo- and Glycerophospholipid Impairment to Select Effective Drugs and Biomarkers for CMT1A. Front Neurol. 2020;11:903.
35. Magyar JP, Martini R, Ruelicke T, Aguzzi A, Adlkofer K, Dembic Z, et al. Impaired differentiation of Schwann cells in transgenic mice with increased PMP22 gene dosage. J Neurosci. 1996;16(17):5351-60.
36. Prior R, Silva A, Vangansewinkel T, Idkowiak J, Tharkeshwar AK, Hellings TP, et al. PMP22 duplication dysregulates lipid homeostasis and plasma membrane organization in developing human Schwann cells. Brain. 2024.
37. Zhou Y, Miles JR, Tavori H, Lin M, Khoshbouei H, Borchelt DR, et al. PMP22 Regulates Cholesterol Trafficking and ABCA1-Mediated Cholesterol Efflux. J Neurosci. 2019;39(27):5404-18.
38. Barnes-Velez JA, Aksoy Yasar FB, Hu J. Myelin lipid metabolism and its role in myelination and myelin maintenance. Innovation (Camb). 2023;4(1):100360.
39. Walczak R, Tontonoz P. PPARadigms and PPARadoxes: expanding roles for PPARgamma in the control of lipid metabolism. J Lipid Res. 2002;43(2):177-86.
40. Zhou J, Mock ED, Al Ayed K, Di X, Kantae V, Burggraaff L, et al. Structure-Activity Relationship Studies of alpha-Ketoamides as Inhibitors of the Phospholipase A and Acyltransferase Enzyme Family. J Med Chem. 2020;63(17):9340-59.
41. Sun Q, Xing X, Wang H, Wan K, Fan R, Liu C, et al. SCD1 is the critical signaling hub to mediate metabolic diseases: Mechanism and the development of its

inhibitors. Biomed Pharmacother. 2024;170:115586.
42. Okamoto Y, Takashima H. The Current State of Charcot-Marie-Tooth Disease Treatment. Genes (Basel). 2023;14(7).
43. Steyer B, Cory E, Saha K. Developing precision medicine using scarless genome editing of human pluripotent stem cells. Drug Discov Today Technol. 2018;28:3-12.
44. Chen L, Zhao ZW, Zeng PH, Zhou YJ, Yin WJ. Molecular mechanisms for ABCA1-mediated cholesterol efflux. Cell Cycle. 2022;21(11):1121-39.
45. Parasassi T, De Stasio G, d'Ubaldo A, Gratton E. Phase fluctuation in phospholipid membranes revealed by Laurdan fluorescence. Biophys J. 1990;57(6):1179-86.
46. Rohwedder A, Zhang Q, Rudge SA, Wakelam MJ. Lipid droplet formation in response to oleic acid in Huh-7 cells is mediated by the fatty acid receptor FFAR4. J Cell Sci. 2014;127(Pt 14):3104-15.
47. Horner SJ, Couturier N, Gueiber DC, Hafner M, Rudolf R. Development and In Vitro Differentiation of Schwann Cells. Cells. 2022;11(23).
48. Buccitelli C, Selbach M. mRNAs, proteins and the emerging principles of gene expression control. Nat Rev Genet. 2020;21(10):630-44.
49. Wilson ER, Della-Flora Nunes G, Weaver MR, Frick LR, Feltri ML. Schwann cell interactions during the development of the peripheral nervous system. Dev Neurobiol. 2021;81(5):464-89.
50. Momenbeitollahi N, Cloet T, Li H. Pushing the detection limits: strategies towards highly sensitive optical-based protein detection. Anal Bioanal Chem. 2021;413(24):5995-6011.
51. Frob F, Bremer M, Finzsch M, Kichko T, Reeh P, Tamm ER, et al. Establishment of myelinating Schwann cells and barrier integrity between central and peripheral nervous systems depend on Sox10. Glia. 2012;60(5):806-19.
52. Arthur-Farraj PJ, Latouche M, Wilton DK, Quintes S, Chabrol E, Banerjee A, et al. c-Jun reprograms Schwann cells of injured nerves to generate a repair cell essential for regeneration. Neuron. 2012;75(4):633-47.
53. Helbling-Leclerc A, Zhang X, Topaloglu H, Cruaud C, Tesson F, Weissenbach J, et al. Mutations in the laminin alpha 2-chain gene (LAMA2) cause merosin-deficient congenital muscular dystrophy. Nat Genet. 1995;11(2):216-8.
54. Kim HS, Lee J, Lee DY, Kim YD, Kim JY, Lim HJ, et al. Schwann Cell Precursors from Human Pluripotent Stem Cells as a Potential Therapeutic Target for Myelin Repair. Stem Cell Reports. 2017;8(6):1714-26.
55. Furlan A, Adameyko I. Schwann cell precursor: a neural crest cell in disguise? Dev Biol. 2018;444 Suppl 1:S25-S35.
56. Lambrichts I, Driesen RB, Dillen Y, Gervois P, Ratajczak J, Vangansewinkel T, et al. Dental Pulp Stem Cells: Their Potential in Reinnervation and Angiogenesis by Using Scaffolds. J Endod. 2017;43(9S):S12-S6.
57. Cavelier C, Lorenzi I, Rohrer L, von Eckardstein A. Lipid efflux by the ATP-binding cassette transporters ABCA1 and ABCG1. Biochim Biophys Acta. 2006;1761(7):655-66.
58. Saher G, Brugger B, Lappe-Siefke C, Mobius W, Tozawa R, Wehr MC, et al. High cholesterol level is essential for myelin membrane growth. Nat Neurosci. 2005;8(4):468-75.
59. Nagao K, Maeda M, Manucat NB, Ueda K. Cyclosporine A and PSC833 inhibit ABCA1 function via direct binding. Biochim Biophys Acta. 2013;1831(2):398-406.
60. Chawla A, Boisvert WA, Lee CH, Laffitte BA, Barak Y, Joseph SB, et al. A PPAR gamma-LXR-ABCA1 pathway in macrophages is involved in cholesterol efflux and atherogenesis. Mol Cell. 2001;7(1):161-71.
61. Mukherjee S, Raghuraman H, Chattopadhyay A. Membrane localization and dynamics of Nile Red: effect of cholesterol. Biochim Biophys Acta. 2007;1768(1):59-66.
62. Yu W, So PT, French T, Gratton E. Fluorescence generalized polarization of cell

membranes: a two-photon scanning microscopy approach. Biophys J. 1996;70(2):626-36.
63. Bai Y, Treins C, Volpi VG, Scapin C, Ferri C, Mastrangelo R, et al. Treatment with IFB-088 Improves Neuropathy in CMT1A and CMT1B Mice. Mol Neurobiol. 2022;59(7):4159-78.
64. Montani L, Pereira JA, Norrmen C, Pohl HBF, Tinelli E, Trotzmuller M, et al. De novo fatty acid synthesis by Schwann cells is essential for peripheral nervous system myelination. J Cell Biol. 2018;217(4):1353-68.
65. Peng K, Sant D, Andersen N, Silvera R, Camarena V, Pinero G, et al. Magnetic separation of peripheral nerve-resident cells underscores key molecular features of human Schwann cells and fibroblasts: an immunochemical and transcriptomics approach. Sci Rep. 2020;10(1):18433.
66. Lutz AB. Purification of schwann cells from the neonatal and injured adult mouse peripheral nerve. Cold Spring Harb Protoc. 2014;2014(12):1312-9.
67. Fregien NL, White LA, Bunge MB, Wood PM. Forskolin increases neuregulin receptors in human Schwann cells without increasing receptor mRNA. Glia. 2005;49(1):24-35.
68. Monje PV. Human Schwann Cells in vitro II. Passaging, Purification, Banking, and Labeling of Established Cultures. Bio Protoc. 2023;13(22):e4882.
69. Sezgin E, Waithe D, Bernardino de la Serna J, Eggeling C. Spectral imaging to measure heterogeneity in membrane lipid packing. Chemphyschem. 2015;16(7):1387-94.

SUPPLEMENTARY METHODS

Spectral analysis of Nile Red using Generalized Polarization (GP) – Nile Red is a lipophilic dye known for its intense fluorescence, which can range from deep red when interacting with polar membrane lipids to vibrant yellow gold when bound to neutral lipids in intracellular storage. Cells were stained with the Nile Red dye (1/600, MedChem Express) for 2 hours, and washed 3x in PBS. SCP were recorded at excitation wavelengths of a maximum of 549 nm and an emission maximum of 628 nm. Spectral imaging values were normalized by subtracting unstained blanks at the excitation, and generalized polarization was calculated as a measure for membrane polarity, ranging from -1 to +1. The GP-values were calculated by using the fluorescence signal intensities I_R and I_B at the red- and blue-shifted emission wavelengths λ_{Ld} (Liquid-disordered, red-shifted) and λ_{Lo} (Liquid-ordered, blue-shifted), respectively (69): $GP = \frac{I_B - I_R}{I_B + I_R}$. The spatial heterogeneity in lipid packing (or GP-values) was measured by recording the whole emission spectrum for each image pixel. For this, a confocal microscope was equipped with a 32-channel gallium arsenide phosphide (GaAsP) detector. By using the custom Fiji/ImageJ plug-in, as previously mentioned, an improved determination of GP-values by modeling the spectral data at each image pixel could be demonstrated, which allows the observation of precise differences in lipid packing (69).

SUPPLEMENTARY TABLES AND FIGURE

Supplementary Table 1: List of abbreviations used throughout this thesis.

Abbreviation	Explanation
CMT	Charcot-Marie-Tooth
SC	Schwann cells
HMSN	Hereditary motor and sensory neuropathy
NCV	Nerve conduction velocities
CMT1	Charcot-Marie-Tooth demyelinating type 1
CMT2	Charcot-Marie-Tooth axonal type 2
CMT1A	Charcot-Marie-Tooth disease type 1A
Mb	Megabase
PMP22	Peripheral myelin protein 22
EMT	Epithelial-to-mesenchymal transition
SCP	Schwann cell precursors
iSC	Immature Schwann cells
Nrg1	Neuregulin 1
Lama2	Laminin-211
Lama4	Laminin-411
cAMP	Cyclic adenosine monophosphate
PKA	Protein kinase activation
MS	MiniMACS separator
GP	Generalized Polarization
DRG	Dorsal root ganglia
KO	Knock-out
ABCA1	ATP-binding cassette transporter A1
CDP	Cytidine diphosphocholine
PC	Phosphatidylcholine
PE	Phosphatidylethanolamine

FASN	Fatty acid synthase
ER	Endoplasmic reticulum
UPR	Unfolded protein Response
GPMV	Giant plasma membrane vesicle
DPSC	Dental pulp stem cell
LD	Lipid droplet
REES	Red edge excitation shift
ApoA	Apolipoprotein
PPARγ	Proliferator-activated receptor γ
MACS	Magnetic-activated cell sorting
PLAAT3	Phospholipase A and acyltransferase 3
PLA1	Phospholipase A1
PLA2	Phospholipase A2
SCD1	Stearoyl-CoA Desaturase 1
MUFA	Monounsaturated fatty acids
ISO	Isogenic
PDGF-bb	Platelet-derived Growth Factor-BB
TALEN	Transcription activator-like effector nucleases
BSA	Bovine serum albumin
PFA	paraformaldehyde
PBS	Phosphate buffered saline
(RT)-qPCR	(Real-time)-Quantitative polymerase chain reaction
λ_{Ld}	Liquid-disordered emission wavelength
λ_{Lo}	Liquid-ordered emission wavelength
GaAsP	Gallium arsenide phosphide
I_R	Red spectrum intensity
I_B	Blue spectrum intensity
FACS	Fluorescence-activated cell sorting
iPSC	Induced pluripotent stem cell

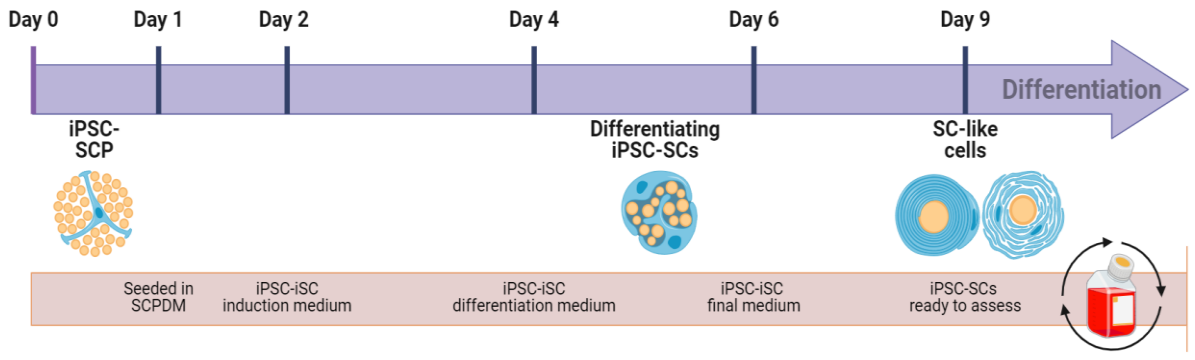

Supplementary Figure 1: Schematic diagram of the iPSC-SCP differentiation process.

Supplementary Table 2: Schwann cell differentiation markers. Functionality and role of the markers *MPZ, p75, Sox10, Oct6, Krox20, Sox2, CD90, NCAM, Lama4, cJun,* and *Cad19* within the differentiation process of Schwann cells.

Marker	Functionality and Role in Differentiation Process
MPZ	**Functionality:** Myelin Protein Zero (MPZ) is a major peripheral nerve myelin structural component. It is involved in forming and stabilizing myelin sheaths in Schwann cells. **Role in Differentiation:** MPZ expression is associated with the maturation of Schwann cells and myelin production. Its presence indicates the progression of Schwann cells towards a more mature, myelinating phenotype.
P75	**Functionality:** The p75 neurotrophin receptor is a signaling receptor for neurotrophins. It plays a role in cell survival, proliferation, and differentiation. **Role in Differentiation:** In the context of Schwann cell differentiation, p75 is often considered a marker for early Schwann cell precursors. It regulates the balance between myelinating and non-myelinating Schwann cell fates.
SOX10	**Functionality:** Sox10 is a transcription factor crucial for neural crest development and the specification of Schwann cell lineage. **Role in Differentiation:** Sox10 is a key regulator of Schwann cell differentiation. It promotes the expression of myelin-related genes and is essential for developing Schwann cells into a myelinating phenotype.
OCT6	**Functionality:** Oct6 (POU3F1) is a transcription factor that belongs to the POU domain family. **Role in Differentiation:** Oct6 is involved in the early stages of Schwann cell differentiation. It regulates the transition of neural crest cells into Schwann cell precursors and is essential for initiating myelination.
KROX20	**Functionality:** Krox20 (EGR2) is a transcription factor regulating myelination in Schwann cells. **Role in Differentiation:** Krox20 is a critical mediator of Schwann cell myelination. Its expression marks the transition from immature Schwann cells to a myelinating phenotype. It regulates the expression of key myelin genes and is necessary for proper myelin sheath formation.
SOX2	**Functionality:** Sox2 is a transcription factor associated with pluripotency and early neural development. **Role in Differentiation:** Sox2 is expressed in neural crest cells and is involved in the early stages of Schwann cell development. It helps specify neural crest cells towards a Schwann cell lineage, but its expression decreases as Schwann cells mature.
CD90	**Functionality:** CD90 (Thy-1) is a glycoprotein involved in cell-cell and cell-matrix interactions, and in the regulation of cell differentiation and adhesion, typically expressed by fibroblasts. **Role in differentiation:** Dysregulation can affect SC adhesion and differentiation, contributing to demyelination.
NCAM	**Functionality:** Neural Cell Adhesion Molecule (NCAM) is involved in neuron-neuron and neuron-glia interactions, important for neural development and regeneration. **Role in differentiation:** Altered expression may disrupt SC-axon interactions and myelination processes in CMT1A.
LAMA4	**Functionality:** Laminin 411 is a component of the extracellular matrix involved in cell adhesion, differentiation, and migration. **Role in differentiation:** Essential for SC differentiation and myelination; abnormalities can contribute to the defective myelination in CMT1A.
CJUN	**Functionality:** Transcription factor involved in regulating SC proliferation, apoptosis, and dedifferentiation. **Role in differentiation:** Elevated levels are associated with SC dedifferentiation and demyelination in CMT1A.
CAD19	**Functionality:** Cadherin 19 is a cell adhesion molecule specific to neural tissues, it is involved in the maintenance of tissue structure and signaling. **Role in differentiation:** Specific marker of SCP. Abnormal expression may impact SC-axon interactions and contribute to the myelination defects in CMT1A.

Supplementary Table 3: Primary and secondary antibodies and dye used for immunocytochemistry.

A) Primary

Target	Host species	Ref. No.	Dilution	Isotype	Manufacturer
MPZ	Rabbit	ab183868	1/250	IgG	Abcam, Cambridge, UK
Sox2	Mouse	sc-365823	1/250	IgG1	Santa Cruz, Texas, USA
Oct6	Rabbit	ab221964	1/250	IgG	Abcam, Cambridge, UK
P75 NTR	Mouse	sc-271707	1/250	IgG1	Santa Cruz, Texas, USA
Krox-20	Rabbit	ab245228	1/250	IgG	Abcam, Cambridge, UK
cJun	Rabbit	ab40766	1/250	IgG	Abcam, Cambridge, UK
ABCA1	Rabbit	ab7360	1/200	IgG	Abcam, Cambridge, UK

B) Secondary

Target	Species	Ref. No.	Dilution	Isotype	Manufacturer
Alexa 488	Goat anti-mouse	A11017	1/300	IgG1	Invitrogen by Thermo Fisher Scientific, Life Technologies Corporation, Oregon, Eugene, USA
Alexa 488	Goat anti-rabbit	A11008	1/300	IgG	
Alexa 555	Goat anti-mouse	A21432	1/300	IgG	
Alexa 555	Donkey anti-rabbit	A31572	1/300	IgG	

C) Dye

Target	Species	Ref. No.	Dilution	Isotype	Manufacturer
Nile Red	/	HY-D0718	1/600	/	MedChemExpress, New Jersey, USA

Supplementary Table 4: List of used primers for qPCR. All primers were humane.

Gene transcript target	Full name	Primer sequences
YWHZ	Tyrosine-3-Monooxygenase/Tryptophan 5-Monooxygenase Activation Protein Zeta	Forward: CTTGACATTGTGGACATCGG Reverse: TATTTGTGGGACAGCATGGA
RPL13A	Ribosomal Protein L13	Forward: AAGTTGAAGTACCTGGCTTTCC Reverse: GCCGTCAAACACCTTGAGAC
Krox20	Early growth response protein 2 (EGR2)	Forward: CCACGTCGGTGACCATCTTT Reverse: TTGATCATGCCATCTCCGGC
Sox10	SRY-box 10	Forward: CCAGGCCCACTACAAGAGC Reverse: GGCTCTGGCCTGAGGGG
MBP	Myelin Basic Protein	Forward: GCCGGACCCAAGATGAAAAC Reverse: CAGTCCTCTCCCCTTTCCCT
MPZ	Myelin Protein Zero (P0)	Forward: TGCTCTTCTCTTCTTTGGTGCT Reverse: AGAAGGAGCAGTGCAGGGT
Lama4	Laminin 411	Forward: CAGTGTAACCGGAGAATGCTTG Reverse:GACGCACTTATCACAGCTTATGG
Sox2	SRY-box 2	Forward: GACCAGCTCGCAGACCTACA Reverse: CTCGGACTTGACCACCGAAC
cJun	Jun-Proto-Oncogene	Forward: ACGGCGGTAAAGACCAGAAG Reverse: CTCGCCCAAGTTCAACAACC
Cad19	Cadherin-19	Forward:TTACTGCTGCGTTTTATGTTGGG Reverse: GCTGGCCGATGTGATGACTA
CD90	Cluster of Differentiation 90 (Thy-1)	Forward: GGATGGCGAGTGACTTAGGG Reverse: TCTCAGTCCTGGATCGGGTT
P75 NTR	Neurotrophin receptor p75	Forward: AGTTGGACTGATTGTGGGTGT Reverse: CAGGCACAAGGGCTTCTTTTT
NCAM	Neural cell adhesion molecule	Forward: TGGGTTCCCCTTGGACTGG Reverse: GCCTGAAGCCCGAAACAAC